ChemElectroChem

Review
doi.org/10.1002/celc.202400278

Chemistry Europe
European Chemical Societies Publishing

www.chemelectrochem.org

Review on Artificial Interphases for Lithium Metal Anodes: From a Mechanical Perspective

Yueying Peng,[a] Ryota Tamate,*[b] and Kei Nishikawa*[c]

Lithium (Li) metal is a promising candidate for next-generation high-energy-density rechargeable batteries. However, the solid electrolyte interphase (SEI) inevitably suffers from mechanical fracture owing to the large morphological change during Li cycling, leading to the uncontrollable growth of Li dendrites, low Coulombic efficiency, and short cycle life. The fabrication of an artificial interphase is an effective strategy for improving the performances of Li metal anodes. The ideal artificial interphase should provide sufficient mechanical robustness to suppress dendritic Li growth and accommodate large volume changes during Li deposition-dissolution cycles. In this review, we focus on the fabrication of mechanically robust artificial interphases for stabilizing Li-metal anodes, including the underlying mechanism of SEI fracture, quantitative requirements for mechanical properties, measurements of mechanical properties, and recent progress in the fabrication of mechanically stable artificial interphases.

1. Introduction

The increasing demand for electric vehicles, consumer electronics, and grid-scale storage has necessitated an urgent need for high-energy-density storage systems. Current rechargeable lithium-ion batteries (LIBs), which use lithium metal oxides as cathodes and graphite as anodes, have reached their limits and cannot meet these escalating demands because of their limited capacity.[1] Employing lithium (Li) metal as an anode material is the cornerstone for advancing the progress of high-energy-density LIBs owing to its ultrahigh theoretical specific capacity (3864 mAh g^{-1}, 10 times of commercial graphite anode) and the lowest potential (−3.04 V, vs. the standard hydrogen electrode).[2] Additionally, Li metal can be paired with non-Li cathode materials such as sulfur, oxygen, or air, allowing the pursuit of advanced batteries with higher energy density.[3] However, the commercialization of Li metal anodes is impeded by issues such as low coulombic efficiency (CE), short cycle life, and safety concerns.[4]

These issues are largely attributed to the formation of an unstable solid electrolyte interphase (SEI) on the Li surface, which is generated by the spontaneous reaction between Li metal and organic electrolytes. This native SEI can serve not only as an electronic insulator but also as an ionic conductor, preventing further reactions between the electrolyte and metallic Li and allowing Li-ion transport for electrochemical deposition/dissolution. However, such spontaneously formed SEI generally suffers from inhomogeneity in terms of components, morphologies (such as thickness and surface roughness), and poor mechanical properties.[5] The structural nonuniformity of the SEI tends to induce uneven Li deposition, and even the generation of dendritic Li, triggering safety hazards such as short circuits or even fires in batteries. The fragile nature of the SEI prevents it from withstanding substantial volume changes during the Li plating/stripping process, leading to repetitive SEI breaks/repairs. The aforementioned dendritic Li formation also exacerbates SEI breakage, resulting in the continuous consumption of both Li metal and the electrolyte. Therefore, the construction of a stable SEI film is crucial for improving the performance of Li-metal anodes.

Strategies for SEI construction can be divided into two directions. One involves modulating the electrolyte formulation by tuning the Li salts, solvent molecules, additives, and concentrations. Another approach is to design an artificial interphase, also called an artificial SEI, artificial interlayer, artificial layer, artificial coating, or artificial protective layer/film/coating. Artificial interphase refers to a favorable composition or specifically designed SEI film built on the surface of the Li metal through chemical reactions or physical methods. This artificial interphase is regarded as a promising direction for enhanced controllability of the SEI component, structure, and morphology. Ideally, the artificial interphase should possess the following features: (1) high ionic conductivity to promote uniform Li-ion transportation, (2) good mechanical stability to prevent dendritic Li growth and accommodate the large volumetric change, (3) electronic insulation to block electron

[a] *Dr. Y. Peng*
International Center for Young Scientists (ICYS)
National Institute for Materials Science (NIMS)
1-1-1 Namiki, Tsukuba, 305–0044, Japan

[b] *Dr. R. Tamate*
Research Center for Macromolecules & Biomaterials
National Institute for Materials Science (NIMS)
1-2-1 Sengen, Tsukuba, 305–0047, Japan
E-mail: TAMATE.Ryota@nims.go.jp

[c] *Dr. K. Nishikawa*
Research Center for Energy and Environmental Materials
National Institute for Materials Science (NIMS)
1-1-1 Namiki, Tsukuba, 305–0044, Japan
E-mail: NISHIKAW.Kei@nims.go.jp

tunneling, and (4) strong adhesion to Li or copper substrate to ensure good contact during cell cycling.[6] In designing artificial interphases, these properties should be considered simultaneously to achieve optimal balance and meet the various operational conditions of Li metal anodes, such as high capacity, high rate capability, high voltage, and high or low temperature.

Numerous recent studies have reviewed artificial interphases. For example, Zhang *et al.* highlighted the importance of fabricating artificial interphases for advanced Li metal anodes.[7] Cui and Bao group proposed three key directions for designing effective artificial interphases: mechanical stability, uniform ion transport, and chemical passivation.[8] Cao and coauthors summarized recent progress on fabricating polymer materials with good ionic conductivity as artificial interphases for Li metal anode.[9] Jagger and Pasta highlighted the importance of simultaneously considering the nanostructure, transport, and mechanical properties of the artificial SEI.[10]

Here, we focus on designing an effective interphase from the perspective of mechanical properties to provide comprehensive guidance for fabricating mechanically robust artificial interphases for Li-metal batteries. Given the strong dependence of the interphase properties on its structure and composition, we begin by summarizing the fundamental studies on native SEI, focusing on its model and the underlying mechanism of SEI fracture (Section 2). Next, the quantitative mechanical parameters required for the stabilization of the Li metal anode are outlined by combining theoretical studies with experimental results (Section 3.1). Subsequently, we discuss how to measure the mechanical parameters using mechanical testing methods (Section 3.2). In Section 4, we summarize the recent progress in the fabrication of mechanically robust artificial interphases, which are divided into three categories: inorganic materials, organic polymer materials, and inorganic/organic hybrid materials. Finally, we offer suggestions for studying the underlying mechanism of SEI fracture, evaluating the mechanical properties, designing mechanically stable artificial interphase materials, and proposing promising avenues for future research in this field.

2. Why we need Artificial Interphase

A typical morphological change on a Li metal anode is shown in Figure 1a. As Li metal is highly reactive, a native SEI is spontaneously generated once it contacts the organic electrolyte. During Li electrodeposition, Li ions pass through the SEI layer, deposit, and grow beneath it, resulting in stress acting on both Li and the SEI.[11] As the Li metal grows, volume expansion occurs, leading to increased stress.[12] When the SEI layer cannot withstand this increased stress, it fractures, triggering a localized Li-ion transfer and dendritic Li growth.[13] Moreover, the freshly exposed Li readily reacts to reform the SEI, increasing the electrolyte consumption and metallic Li loss. Therefore, the construction of a mechanically stable interphase is crucial for enhancing the cycling performance of Li metal anodes.

The structure, composition, and spatial distribution of the SEI significantly influence the Li-ion transport process, uniformity of stress generation, and mechanical properties. Therefore, we first briefly introduce the SEI structural model and its mechanical properties. We then specifically discuss the process of SEI fracture, including stress generation, deformation of both SEI and Li and its impact on Li deposition.

2.1. Solid Electrolyte Interphase Models and Properties

Although the concept of the SEI was introduced by Peled in the 1970s,[17] it continues to be the most crucial yet least understood part in the realm of rechargeable Li-ion batteries.[18] This complexity arises from its intricate constituents, which are affected by many factors, such as the electrolyte, current

Dr. Yueying Peng is a research fellow at the International Center for Young Scientists (ICYS) at the National Institute for Materials Science (NIMS). She received her Ph.D. in physical chemistry from Xiamen University, China, in 2019. Her research interests focus on developing advanced energy storage batteries, particularly lithium metal-based batteries.

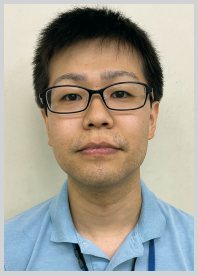

Dr. Ryota Tamate is an independent scientist of Research Center for Macromolecules & Biomaterials at the National Institute for Materials Science (NIMS) in Japan. He received his BS and MS degrees from Kyoto University. After working at Bridgestone Co., he received a Ph.D. degree in 2016 from the University of Tokyo under the supervision of Professor Ryo Yoshida. Following this, he worked as a JSPS Postdoctoral Fellow under Professor Masayoshi Watanabe at Yokohama National University. Since 2019, he has held his current position at NIMS. His research interests include functional soft materials for energy applications.

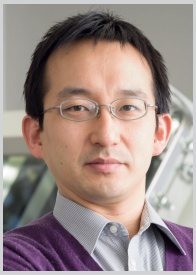

Dr. Kei Nishikawa is a principal researcher at Research Center for Energy and Environmental Materials in the National Institute for Materials Science (NIMS). He received his Ph.D. in energy science from Kyoto University, Japan in 2006. He worked as postdoctoral researcher in Tokyo Metropolitan University (2007), École Polytechnique (2008–2009), Japan Aerospace Exploration Agency (2009–2011), and NIMS (2011–13) for battery materials research. His research interests are Li metal batteries, electrodeposition of metal, and mass transfer phenomenon in electrochemical systems.

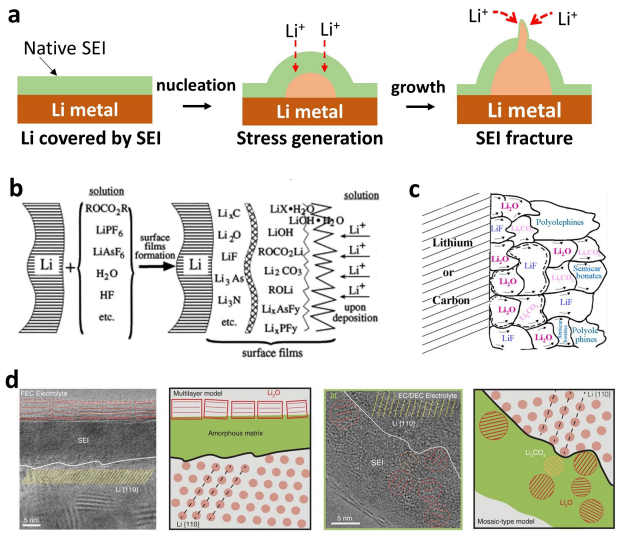

Figure 1. (a) Illustration of Li growth process. (b) Multilayer model for SEI. Reproduced with permission.[14] Copyright 2000 Elsevier. (c) Mosaic model for SEI. Reproduced with permission.[15] Copyright 2017 IOP Publishing. (d) Cryo-transmission electron microscopy (TEM) images of SEI at atomic resolution. Reproduced with permission.[16] Copyright 2017 American Association for the Advancement of Science.

density, potential, temperature, and electrode surface. Several models have been developed to describe the composition and structure of the SEI layers. Aurbach *et al.* analyzed the chemical structure and morphologies of the surface film formed on Li metal anode through X-ray photoelectron spectroscopy (XPS), Fourier transform infrared (FT-IR) spectroscopy, scanning electron microscopy (SEM), and atomic force microscopy (AFM).[19] Based on the results, they proposed a multilayer SEI model (Figure 1b).[13,14,20] The compact inner layer, close to the Li electrode, is dominated by low oxidation inorganic compounds such as Li_2O, Li_xC, LiF, Li_3N. The porous outer layer near the electrolyte side is mainly composed of organic compounds such as $ROCO_2Li$, ROLi, and $(CH_2OCO_2Li)_2$, which are highly dependent on the solvents. Based on the experimental results of Aurbach *et al.*, Peled *et al.* further proposed the mosaic SEI model (Figure 1c).[15] Similar to the multilayer model, the SEI is fundamentally composed of two layers: an inorganic-rich inner layer and an organic-rich outer layer. The model assumes that each component creates a separate microphase that contributes to the construction of a mosaic-type SEI. Both multilayer SEI and mosaic models have been widely accepted and validated.[21] In particular, recently developed cryo-electron microscopy enables visualization of the SEI structure at atomic resolution. A mosaic-type SEI was found in the commonly used electrolyte of 1 M $LiPF_6$ in ethylene carbonate/diethyl carbonate (EC-DEC), whereas a multilayered SEI structure was observed after the addition of a fluoroethylene carbonate (FEC) additive (Figure 1d).[16]

The structure and composition of the SEI present an inhomogeneous distribution in both planar and vertical orientations, leading to inhomogeneity in the mechanical properties. By combining experimental measurements with computational studies, Shin *et al.* determined Young's moduli of the individual components in the SEI, following the order LiF (58.1 GPa) > Li_2CO_3 (36.2 GPa) > Li_2EDC (21.6 GPa) > LiMC (10.5 GPa) > LiEC (7.3 GPa) > PEO (2.4 GPa).[22] The quantified results demonstrate the nonuniform mechanical properties of the SEI in the vertical direction, with an internal stiffer inorganic layer and an external softer organic layer. In addition, the morphology and structure of SEI on the Li surface undergo dynamic changes during cycling, rendering their mechanical properties more complex and variable. Wolff *et al.* employed in-situ AFM to investigate the mechanical evolution of SEI on Li metal anodes.[23] The stiffness of the SEI on the Li surface was heterogeneous, and its mean value gradually increased with increasing storage time in the electrolyte. During Li deposition, Sacci *et al.* revealed the nonuniform distribution of the SEI in both the planar and vertical directions and found that its thickness gradually increased with increasing Li deposition capacity.[24] The uneven distribution of the SEI thickness leads to subsequent uneven Li dissolution, as Li metal is more prone to dissolution from thin SEI areas.[25]

2.2. Facture Mechanism of Solid Electrolyte Interphase

Understanding the mechanical failure mechanisms of SEIs is beneficial for creating effective artificial interphases. During Li deposition, Li nucleation and growth occurred at the Li/SEI interface. As metallic Li expands in volume, the upper SEI layer constrains the growth of Li beneath it, resulting in stress acting on both the SEI and the Li metal (Figure 2a). Owing to the uncontrollable nature of Li growth, the stress exerted on the SEI layer is highly complex, originating from various directions and changing dynamically. To simplify the study, it is assumed that the SEI experiences tensile stress, whereas metallic Li bears compressive stress.[29]

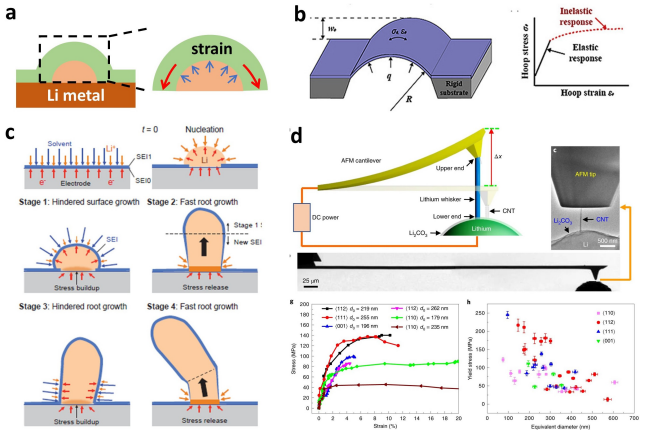

Figure 2. (a) Li growth at SEI/Li interface and tensile strain of SEI (the blue arrows represent the direction of Li growth, while the red arrows stand for the direction of SEI strain). (b) Schematic of the deflected free-standing membrane under a uniform lateral pressure and hoop stress-strain relationship. Reproduced with permission.[26] Copyright 2020 Elsevier. (c) Schematic of the base growth model for Li whiskers. Reproduced with permission.[27] Copyright 2017 Elsevier. (d) Schematic of the AFM-ETEM setup, stress-strain curves, and the yield stress that varies with an equivalent diameter of Li whiskers. Reproduced with permission.[28] Copyright 2020 Springer Nature.

To reveal the underlying mechanism of SEI fractures, it is necessary to investigate how much stress acts on the SEI layer and how the SEI responds to stress. It has been demonstrated that preferential Li deposition or dissolution occurs in morphologies with highly curved surfaces (such as dendrites, dips, and irregular geometry)[30] and surfaces with defects (such as cracks, impurities, pores, grain boundaries, and slip lines),[31] inducing the generation of significant local stress. This suggests that fabricating an artificial interphase with a uniform structure to promote uniform Li deposition with a densely deposited Li morphology is necessary to decrease localized stress generation. To accurately measure the mechanical behavior of a thin SEI film, Yoon *et al.* employed a free-standing membrane to avoid the influence of the substrate and an inaccurate contact area (Figure 2b).[26] Combining the AFM images and membrane bulge configurations, they identified the elastic and inelastic responses of the SEI layer. The elastic limit of the SEI was ~3.8%, and cracking began soon after entering the inelastic regime, with serious degradation at a strain of ~5.6%. Thus, the inelastic regime was attributed to a combination of plastic deformation and crack evolution. The addition of FEC enhanced the resistance to SEI fracture, resulting in a few cracks at a high strain of 6.2%.

In addition to the mechanical behaviors mentioned above, mechanical stress also impacts Li electrodeposition ($Li^+ + e \rightarrow$ Li), and the SEI fracture will trigger a chemical reaction between metallic Li and electrolyte to produce a new SEI layer (Li + electrolyte→SEI). To reveal such electro-chemo-mechanical mechanisms, various in situ or operando technologies have been developed to monitor the process of Li deposition in real-time, such as in situ optical microscopy,[32] in-situ AFM,[23,33] in situ transmission electron microscopy (TEM),[12b,29] and in situ AFM with an environmental transmission electron microscope (AFM-ETEM).[28,34]

For example, Kushima *et al.* developed an in-situ ETEM to observe the Li growth process.[29] They incorporated a chemical reaction between Li and electrolyte (Li + electrolyte→SEI) and calculated the Li growth rate during electrodeposition. Four stages were identified in Li electrodeposition (Figure 2c). In stage 1, spherical Li nuclei formed and expanded beneath the SEI layer, with their diameter increasing proportionally with the square root of time, suggesting a diffusion-controlled growth process. During stage 2, the SEI layer failed to withstand stress, resulting in fractures along the sides near the root. Li preferentially grew through the thin SEI layer and extended upward to create whiskers characterized by rapid lengthening while maintaining a constant width. In stage 3, a decreased Li growth rate was observed, which was attributed to new SEI formation/thickening. Stage 4 revealed the emergence of a kink, with a new segment originating from the root exhibiting increased length and width, while the previously formed segment remained unaltered.

To simultaneously achieve real-time observation and stress measurement, He *et al.* used AFM-ETEM to capture the force change during the Li nucleation and growth process.[34b] They also demonstrated that Li undergoes slow nucleation and early growth, followed by fast whisker growth, and finally, four possible behaviors of the Li whiskers were observed: bucking, widening, kinking, or yielding. Importantly, they observed that the vertical growth of Li whiskers was prevented when the constrained force reached a certain value. However, the critical stress value could not be estimated because multiple whiskers existed simultaneously. To achieve this, Zhang and colleagues improved the AFM-ETEM setup using an arc-discharged multi-wall carbon nanotube (CNT), successfully capturing an individual Li whisker (Figure 2d).[28] The elastic-plastic phenomena during Li growth were monitored, showing elastic strain with a limit of less than 4% and plastic strain reaching up to 20%. In addition, they found that smaller Li whiskers generate higher yield stress, reaching 244 MPa, which is much higher than that of bulk Li metal[35] and micro-sized Li.[36] Their experiment once again confirmed that metallic Li primarily undergoes elastic deformation, followed by plastic deformation, and generates large stress during Li whisker growth.

In summary, the spontaneously formed SEI, with its inhomogeneous structure, inevitably undergoes breakdown owing to its susceptibility to localized stress as well as its poor mechanical properties, rendering it unable to withstand large stress variations during Li deposition. Thus, fabricating artificial interphases with controllable structures and desirable mechanical properties is a promising strategy for achieving stable cycles for advanced Li metal batteries.

3. Mechanical Properties of Solid Electrolyte Interphase

3.1. Requirements for the Mechanical Properties of Solid Electrolyte Interphase

The growth of Li dendrites induces significant stress.[28] Thus, suppressing dendritic Li growth is the primary requirement for avoiding SEI fracture. Newman *et al.* developed valuable mathematical models to understand the Li growth process by incorporating factors such as thermal behaviors,[43] ion transport,[44] and surface energy.[45] As a pioneering effort, Monroe and Newman first introduced the impact of mechanical forces into Li kinetics models.[46] Three factors – elasticity, viscosity, and pressure – were examined, demonstrating their notable effects on exchange current densities and potentials. To further simplify the model, Monroe and Newman focused solely on elastic deformation and investigated the effect of electrolyte elasticity, with different Poisson's ratio (ν^s) and shear modulus (G^s), on the Li/electrolyte interfacial stability (Figure 3a).[37] In a typical polymer matrix of poly(ethylene oxide) (PEO) ($\nu^s = 0.33$), the dendritic Li growth can be mechanically inhibited when its shear modulus is approximately ~6.8 GPa, which is twice that of metallic Li (~3.4 GPa). An incompressible electrolyte ($\nu^s = 0.5$) can realize a stable interface when $G^s/G^e = 1$, while it is difficult to achieve interfacial stability for a completely compressible electrolyte ($\nu^s = 0$). This implied that a higher shear modulus is required for compressible electrolytes compared to incompressible electrolytes. Many studies have

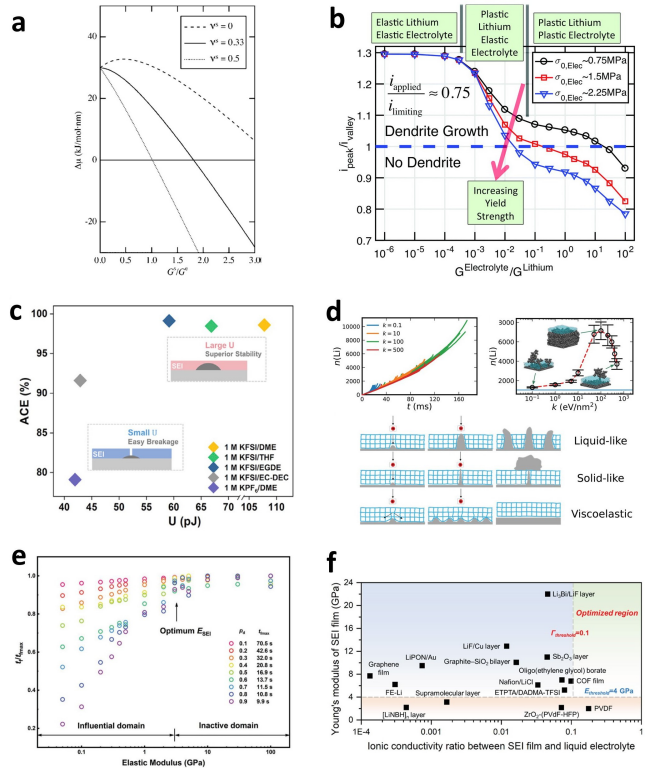

Figure 3. (a) Interfacial stability varies with electrolyte shear modulus and Poisson's ratio. Reproduced with permission.[37] Copyright 2005 IOP Publishing. (b) Current varies with electrolyte shear modulus for different yield strengths of the electrolytes. Reproduced with permission.[38] Copyright 2017 Royal Society of Chemistry. (c) Relationship between average Coulombic efficiency and maximum elastic deformation energy (U) of the SEIs. Reproduced with permission.[39] Copyright 2021 Elsevier. (d) Number of deposited Li various with bond strength between polymer bead and mobility of polymer bead, and schematic of the effects of polymer mechanical properties. Reproduced with permission.[40] Copyright 2020 Wiley-VCH. (e) Failure times vary with different SEI elastic modulus (E_{SEI}) and structural uniformity (p_d). Reproduced with permission.[41] Copyright 2020 Wiley-VCH. (f) Comparison of Young's modulus and ionic conductivity for effective SEI. Reproduced with permission.[42] Copyright 2022 Wiley-VCH.

confirmed the existence of high-modulus theoretical models. For example, combined with time-resolved hard X-ray microtomography, McDonald *et al.* found that increasing the electrolyte modulus helps suppress the vertical growth of Li dendrites through current delocalization.[47] Driven by theoretical predictions, materials with high moduli, such as ceramics,[48] and carbon-based materials,[49] have been widely explored as artificial interphases, and their efficiency in promoting uniform Li deposition has been demonstrated.

Notably, the linear elasticity theory was employed in the model discussed above, limiting the study of very small strain situations, such as initial Li nucleation and early growth. However, actual battery systems are more complex, with nonlinear elastic deformation, plastic deformation, stress relaxation, local deformation, and mechanical fractures. Thus, many experimental and computational studies have been conducted to supplement and refine the mechanical stress-induced effects on the kinetics of Li deposition.

In a later study, Newman *et al.* discovered that an extremely stiff separator induces both elastic and plastic deformation within Li, resulting in a flat Li electrode.[50] Barai *et al.* further confirmed that elastic and plastic deformation of both Li and polymer occurs in an electrolyte with a high shear modulus.[38] As shown in Figure 3b, increasing the yield strength of the electrolyte inhibits dendritic protrusions. Mukherjee *et al.* also incorporated the elastic-plastic effects on dendritic Li growth in an all-solid-state Li battery.[51] Their results showed that increasing the fracture toughness of the solid electrolytes could prevent Li dendrite penetration. The above elastic-plastic analysis suggests that the elastic modulus alone may not be sufficient to assess the stability of the SEI layer, and the yield strength and fracture toughness should also be considered.

Another factor contributing to increased stress is volume expansion. With the increased capacity of the deposited Li, volume expansion inevitably occurs, leading to a dramatic stress increase in the Li anode.[12a] Thus, a mechanically robust artificial interphase is required to accommodate large volume changes. Liu *et al.* demonstrated that employing a soft separator accommodated a substantial volume change through elastic deformation and conformal interfacial motion.[52] Zhang *et al.* found that employing the parameter of the maximum elastic deformation energy (U), the combined effects of Young's modulus and elastic strain, allowed for a more accurate assessment of the stability of the SEI layer compared to using the elastic modulus alone (Figure 3c).[39] Their results suggested that a high U-value in the SEI layer enables it to absorb all the energy from anode expansion via elastic deformation, preventing energy from triggering SEI fracture, and thus significantly improving stability.

Furthermore, the Li nucleation exhibits heterogeneous behavior, randomly occurring in certain regions and causing local stress, which triggers further deposition and dendritic Li growth.[53] An effective artificial interphase should possess the capability to adapt to these heterogeneous variations. To quantify such adaptability, Kong *et al.* introduced the relaxation time parameter coupled with the stiffness of the coated polymer layer to simulate Li deposition dynamics.[40] The simulation results revealed that optimal stiffness and relaxation time exist to ensure uniform Li deposition, which can be achieved by simultaneously optimizing both the bond strength between the polymer beads and the mobility of the polymer beads (Figure 3d). Viscoelastic polymers exhibit mechanical robustness over short timescales while demonstrating adaptability over longer durations, offering an optimal blend of flexibility and strength for an artificial layer. It has been experimentally demonstrated that viscoelastic materials serve as an exceptional adaptive interfacial layer for Li metal anodes, capable of reversibly transitioning between their "liquid" and "solid" properties, thereby hindering Li dendrite growth and improving the electrochemical performance of Li anode.[54]

In addition to the mechanical properties, the Li growth process is also influenced by other properties of the SEI layer, such as structural uniformity, ionic conductivity, dielectric permittivity, surface energy, thickness, and test conditions such as current density and external pressure.[11a,41,42,55] For example,

Zhang *et al.* investigated the effects of the mechanical strength and structural uniformity of SEI on Li dendrite growth.[41] They found that a stable SEI layer without fracture could be realized when the elastic modulus increased to 3.0 GPa. For a lower elastic modulus, increasing structural uniformity is an effective way to improve the stability of the SEI (Figure 3e). Xiong *et al.* considered the influence of both mechanical strength and ionic conductivity of SEI on the Li electrochemical process.[42] Based on electro-chemo-mechanical modeling, they found that the SEI with low ionic conductivity tends to induce localized stress. Though increasing Young's modulus (E) of SEI leads to mitigating the stress concentration, too high values ($E \geq 5$ GPa) cause inefficient Li deposition. Consequently, a moderate Young's modulus ($E \approx 4$ GPa) and high ionic conductivity ($\sigma_{SEI}/\sigma_{electrolyte} > 0.1$) are suggested to achieve a uniform Li deposition (Figure 3f). In a scenario different from the research by Monroe and Newman, Barai *et al.* indicated that dendritic Li suppression can be realized by applying low current densities, regardless of the elastic modulus of the electrolyte.[11a] Further considering the impact of external pressure in a later work, they revealed that applying an appropriate pressure suppress dendritic Li growth. The critical value of external pressure highly depends on the elastic modulus of the electrolyte. This means that rigid solid ceramic electrolytes are much more effective at suppressing dendritic Li growth compared to liquid and soft polymer electrolytes.[55b]

In summary, an effective artificial interphase should possess the following favorable mechanical properties: (1) sufficient elastic modulus and mechanical strength to inhibit dendritic Li growth, (2) effective mechanical flexibility to accommodate significant volume changes, and (3) self-adaptive ability to different morphological changes in different regions when local Li deposition occurs. Furthermore, the Li plating/stripping behaviors is also influenced by other factors such as ion conductivity, structural uniformity, and testing conditions. Therefore, when determining the critical values for the mechanical properties of SEIs, various factors must be comprehensively considered.

3.2. Mechanical Evaluation of Solid Electrolyte Interphase

To evaluate their mechanical characteristics, materials for artificial interphases are typically tested either as self-standing films or as coatings/in-situ formations on the substrates. Here, we mainly discuss four commonly used methods: tensile tests,[59] rheological studies,[54a] AFM-based technology,[33,60] and nanoindentation.[61]

Tensile testing is a fundamental mechanical evaluation method employed to assess the ability of a material to endure applied tensile forces until it fractures. Tensile testing can be used for a wide range of materials, such as metals,[62] polymers,[63] and ceramics[64]. In a typical uniaxial tensile test, a specimen is placed between two tensile clamps and pulled at a constant speed until it reaches the point of fracture. The mechanical responses of the specimens at each point are recorded to plot stress–strain curves. A typical stress–strain curve for a material that shows elastic and plastic deformation is shown in Figure 4a. The stress–strain curve allowed us to identify the elastic deformation, plastic deformation, yield point, and fracture point (or breaking point). In the elastic region, the material can return to its original shape upon the removal of stress, whereas in the plastic region, it undergoes permanent changes in shape. The endpoint of the elastic region is called the yield point, and the corresponding stress is the yield stress or strength. The maximum stress that the sample can withstand before breaking is called the ultimate tensile strength or simply the tensile strength. Fracture strain and stress are evaluated from the fracture point. The area under the stress–strain curve represents the toughness. In the initial linear elastic deformation, the slope can be calculated to obtain Young's modulus (stress/strain). The obtained parameters can be used to assess the mechanical strength and flexibility of the materials as artificial interphases.

Rheological studies are commonly employed to analyze the viscoelastic properties of polymeric materials. Viscoelastic materials exhibit both viscous (fluid-like) and elastic (solid-like) responses under mechanical input, and this characteristic is demonstrated to be helpful to both suppress Li dendritic growth and accommodate the large volume change.[54a] Thus, increasing attention has been paid to developing viscoelastic materials as artificial interphases for Li metal anodes.[54b] The frequency-dependent small amplitude oscillatory shear (SAOS) measurement is widely used to investigate the viscoelastic properties.[56] As shown in Figure 4b, the storage modulus (G') and loss modulus (G'') are analyzed from the stress–strain relationship obtained from SAOS measurements. If G' is greater than G'', solid-like behavior is dominant under the experimental conditions. Conversely, if G'' surpasses G', the material predominantly exhibits viscous liquid-like behavior.

AFM is an advanced probe microscope based on scanning tunneling microscopy (STM). It is widely employed for nanomechanical analysis because of its high spatial resolution and precise force-detection abilities. The basic principle of AFM is its ability to measure the tip–surface interaction by analyzing the displacement of the cantilever amplified by a laser beam system

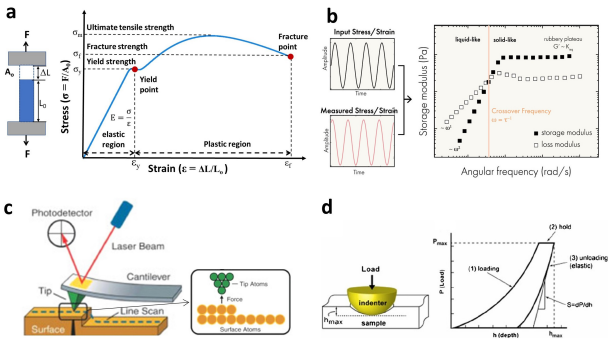

Figure 4. (a) A typical stress-strain curve for a material that shows elastic-plastic deformation under a uniaxial tensile test. (b) Illustration for small amplitude oscillatory shear measurement. Reproduced with permission.[56] Copyright 2021 American Chemical Society. (c) Schematic of the AFM. Reproduced with permission.[57] Copyright 2008 Elsevier (d) Schematic illustration of nanoindentation. Reproduced with permission.[58] Copyright 2013 Springer Nature.

(Figure 4c).[57] AFM can be operated in multiple modes, enabling the simultaneous mapping of both mechanical and morphological features, such as elasticity, viscosity, force, adhesion, hardness, surface roughness, and thickness.[66] However, it is challenging to obtain accurate mechanical parameters of the SEI on Li metal anode owing to its heterogeneous structure, low thickness, and rough surface. Numerous methods have been proposed to improve the precision of mechanical measurements, including AFM-based nanoindentation,[67] amplitude modulation-frequency modulation (AM-FM),[68] quantitative nano-mechanical AFM (QNM-AFM).[69] In particular, the development of in situ/operando AFM techniques allows the observation of the dynamic evolution of the SEI layer on Li metal during the discharging/charging process.[23,33]

Nanoindentation is another popular technique for measuring the mechanical properties of various materials at the nanoscale, such as thin films, coatings, and nanoparticles. In nanoindentation tests, the indenter is pressed into a sample. As shown in Figure 4d,[58] a typical procedure involves increasing the load steadily, holding it, and then releasing it. Throughout the test, the applied load and indentation depth is logged to create a load-displacement curve. The contact area between the indenter and the sample can be calculated using the indenter's as-known radius and the measured indentation depth, which is further used to calculate mechanical parameters such as hardness, elastic modulus, reduced modulus, and stiffness.[61]

While the aforementioned testing methods can offer quantitative mechanical parameters, challenges persist in evaluating the mechanical properties of artificial interphase materials on Li anodes. Firstly, mechanical properties are generally not independent, making it quite difficult to assess the contribution of each mechanical factor to battery performance.

As an artificial interphase material, it is desirable that the material possesses both mechanical strength to inhibit dendritic Li growth and high mechanical flexibility to accommodate significant volume changes. The mechanical strength is usually assessed through metrics such as elastic modulus, tensile strength, stiffness, and nanoindentation hardness. Mechanical flexibility can be evaluated by the elastic deformation region and fracture strain. To assess their suitability as artificial interphase materials more effectively, multiple mechanical factors need to be considered. For example, it was suggested that the maximum elastic deformation energy, combined with the impacts of both Young's modulus and the elastic strain limit, be used to better evaluate the mechanical stability of the SEI.[39]

Another challenge is the accurately measuring the mechanical properties. The mechanical properties of the fabricated artificial interphases materials are typically evaluated either as coatings/in-situ layers on substrates (Li, Cu, or others) or as self-standing films. To ensure the accuracy of the test results, special attention should be paid to the influence of the substrate, surface roughness, thickness, fabricated specimens without defects, and test conditions (such as tips, temperature, and strain rate).[70] For example, AFM and nanoindentation tests are popularly conducted for the artificial interphase materials in-situ formed or coated on substrates. In this case, the influence of surface roughness and the underlying substrate cannot be ignored. Nix *et al.* suggested that nanoindentation data are valid only at depths below 10% of the total film thickness when dealing with a hard film applied to a soft substrate.[71] Although some artificial interphase materials can be fabricated as self-standing films for direct tensile testing and rheological measurements, the results of bulk material may not match the mechanical properties of the thin coating on the electrode.[72] Addressing these challenges involves developing and refining techniques that can provide accurate, reproducible measurements of the mechanical properties.

4. Progress on Fabricating Mechanically Stable Artificial Interphase

To date, various materials have been explored as artificial interphases for Li metal anodes to improve their mechanical stability. Table 1 compares the reported artificial interphases for Li metal anodes in terms of fabrication methods, mechanical properties, and electrochemical performance. We summarize the reported materials and categorize them into three types: inorganic, organic polymer, and inorganic/organic hybrid materials.

4.1. Inorganic Materials

Inorganic materials are popularly employed as artificial interphase materials, primarily because of their outstanding mechanical rigidity and effective suppression of dendritic Li growth. Additionally, inorganic materials generally exhibit high ionic conductivity, which promotes fast ion transport and high stability. Table 2 lists commonly used inorganic materials, including lithium fluoride (LiF),[73,75] lithium nitride (Li_3N),[103] lithium phosphate (Li_3PO_4),[78,79,97] lithium phosphorus oxynitride (LiPON)[74,104], and aluminum oxide (Al_2O_3).[48a,80] As discussed above, mechanical strength is not the sole criterion for judging a good artificial interphase material. To obtain a mechanically robust SEI, other factors should also be considered, such as mechanical flexibility, Li-ion diffusivity, electronic insulation, and (electro)chemical stability.

LiF has been widely demonstrated as one of the most effective SEI species,[105] which can be attributed to a combination of various properties, including high modulus,[22,106] high interfacial energy (Figure 5a),[91] high electron tunneling barrier,[92] and outstanding electrochemical stability.[93] Density functional theory (DFT) calculation showed that LiF exhibits high interfacial energy (73.28 meV $Å^{-2}$) and the ability to suppress Li dendrite follows the order of LiF > Li_2CO_3 > Li_2O > LiCl > Li_2S.[91] The high electron tunneling barrier of LiF makes it efficiently block electron tunneling with lower critical thickness (20.3 Å) than those of Li_3PO_4 (21.6 Å) and Li_2CO_3 (30.2 Å).[92] Fan *et al.* directly deposited LiF film with tunable thickness on Li

Table 1. Comparison of electrochemical performances of artificial interphases for Li metal anodes.

Compositions	Fabrication methods	Mechanical properties	Electrochemical performances		
			Current (mA cm^{-2})	capacity (mAh cm^{-2})	cycling
LiF[73]	Magnetron sputtering	–	1	1	Li/Li cell: 160 h
			0.4	–	$Li/Li_4Ti_5O_{12}$ cell: 500 cycles
LiF/LiPON[74]	Magnetron sputtering	Young's modulus of 90 GPa	0.64	2.5	Li/Cu cell: 320 cycles
			0.64	~2.2	$Cu/LiFePO_4$ cell: 100 cycles with capacity retention of 66%
LiF/Li_3Sb[75]	Dip coating	–	20	2	Li–Li cell: 1306 cycles
			1.3	10	Li/Sulfur cell: 60 cycles with capacity retention of 91.5%
Li_3N[76]	In-situ chemical reaction	–	0.8	0.8	$Li/Li_4Ti_5O_{12}$ cell: 500 cycles
Li_3N-Li_2S/graphene oxide (GO)[77]	Molten Li infusion	Young's modulus of 7.6 GPa	1	1	Li/Li cell: 450 h
			0.765	1.53	$Li/LiNi_{0.8}Mn_{0.1}Co_{0.1}O_2$ cell: 100 cycles with capacity retention ~61%
Li_3PO_3 [78]	In-situ chemical reaction	Young's modulus of 10~11 GPa	0.5	1	Li/Li cell: 600 h
			0.265	0.53	$Li/LiFePO_4$ cell: 200 cycles with capacity retention of 52%
Li_3PO_4 [79]	Magnetron sputtering	-	0.5	0.5	Li/Li cell: 900 h
			0.83	–	Li/Sulfur cell: 200 cycles with capacity retention of 66%
Al_2O_3[80]	Atomic layer deposition (ALD)	–	1	1	Li/Li cell: 240 h
			1	1	Li/Cu cell: 130 cycles
Poly((*N*-2,2-dimethyl-1,3-dioxolane-4-methyl)-5-norbornene-*exo*-2,3-dicarboximide)[81]	Drop casting	Elastic modulus of 0.37 GPa	0.5	1.0	Li/Li cell: 300 h
			0.5	1.0	Li/Cu cell: 200 cycles
Poly(oligo(ethylene glycol) methyl ether methacrylate)-grafted, hypercrosslinked poly(4-chloromethylstyrene) nanospheres (*x*PCMS-*g*-PEGMA)[82]	Drop casting	Elastic modulus of 1.01 GPa Fracture stress of 5.5 MPa Fracture strain of ~20.5% Toughness of 926.7 KJ m^{-3}	10	10	Li/Li cell: 2800 h
			0.4	2	$Li/LiFePO_4$ cell: 100 cycles with capacity retention of 94%
Chitosan/dibenzaldehyde-terminated telechelic poly(ethylene glycol) (CS/DF-PEG-DF)[83]	Drop casting	Mechanical strength of 1.0 GPa Fracture strain of 18.5% Fracture stress of ~3 MPa	10	10	Li/Li cell: 3200 h
			1.7	3.4	$Li/LiFePO_4$ cell: 100 cycles with capacity retention of 60.1%
Poly(methyl methacrylate-*r*-methacrylic acid-*r*-*N*-methylmethacrylamide) (P(MMA-*r*-MAAc-*r*-NMMAm)) based gel electrolyte[84]	Spin coating	Young's modulus of 4.5 MPa Fracture strain of 769% Fracture stress of 5.3 MPa Toughness of 16 MJ m^{-3}	0.5	0.5	Li/Li cell: 1000 h
			0.2	2	$Li/LiNi_{0.6}Mn_{0.2}Co_{0.2}O_2$ cell: 100 cycles with capacity retention $>80\%$
Silly putty, primarily composed of polydimethylsiloxane (PDMS) cross-linked by transient boron-mediated cross-links[54a]	Blade coating	Viscoelastic property	0.5, 1	1.0	Li/Cu cell: 120 cycles
Polyrotaxane-*co*-polyacrylic acid (PR-PAA)[85]	N.A.	Fracture stress of ~0.4 MPa Fracture strain of 800% Self-healing ability	1	1, 4	Li/Li cell: 670 h
			1.5	3	$Li/LiFePO_4$ cell: 100 cycles with capacity retention of 94.8%

Table 1. continued

Compositions	Fabrication methods	Mechanical properties	Electrochemical performances		
			Current (mA cm^{-2})	capacity (mAh cm^{-2})	cycling
Poly(ethylene oxide) /ureido-pyrimidinone (PEO-UPy)[86]	Drop casting	Self-healing ability	1, 5	10	Li/Li cell: 1000 h
			1.44	~1.44	$Li/LiNi_{0.6}Mn_{0.2}Co_{0.2}O_2$ cell: 200 cycles with capacity retention 84.20%
Cu_3N + styrene butadiene rubber (SBR)[61b]	Drop casting	Elastic modulus of 0.81 GPa	1	1	Li/Cu: 100 cycles
			1.5	3	$Li/Li_4Ti_5O_{12}$: 90 cycles with CE of 97.4%
LiF/poly(vinylidene-*co*-hexafluoropropylene) (PVDF-HFP)[87]	Sandwiched between Li and separator	Young's modulus of 6.72 GPa	2.0	1	Li/Li cell: 200 h
			0.375	0.75	$Li/LiFePO_4$ cell: 250 cycles with capacity retention of 80%
LiAl-FBD (FBD: 2,2,3,3-tetrafluoro-1,4-butanediol)[88]	Dip coating	Young's modulus of 30~40 GPa Hardness of ~2 GPa	1	1	Li/Li cell: 1000 h
			0.6	2	$Li/LiNi_{0.5}Mn_{0.3}Co_{0.2}O_2$ cell: 200 cycles with capacity retention ~60%
SiO_2@polydopamine (PDA)[89]	In-situ chemical reaction	Elastic Modulus of 214.98 GPa	5	1	Li/Li cell: 2800 h
			1.5	3	$Li/LiCoO_2$ cell: 300 cycle with capacity retention 79%
Li_3PO_4/polyphosphoric ester (PPE)[90]	Dip coating	Young's modulus of 550 MPa (organic layer) and 12 GPa (inorganic layer)	1	1	Li/Li cell: 2000 h
			0.51	0.51	$Li/LiFePO_4$ cell: 300 cycles with capacity retention of 83.2%

Table 2. Common inorganic materials used as artificial interphase on Li anode.

Inorganic materials	Young's modulus (GPa)	Other properties
LiF	135.3 (crystalline),[22] 58.1 (amorphous),[22]	High interfacial energy[91] Low electronic conductivity[92] High stability against Li[93]
Li_3N	~120,[94]	High ionic conductivity (10^{-3} ~10^{-4} S cm^{-1})[95] Low electronic conductivity[95a] High stability against Li metal[93,96]
Li_3PO_4	10–11,[78] 10.1[97]	High ionic conductivity (10^{-8} S cm^{-1})[78–79] High stability against Li metal[78]
LiPON	33,[98] 77 (elastic modulus),[99] 79,[100]	High ionic conductivity (10^{-6} ~10^{-8} S cm^{-1})[74,101]
Al_2O_3	344.3 ± 15.2 (κ-Al_2O_3),[102] 392.5 ± 44.0 (α-Al_2O_3),[102] 183.2 (amorphous),[102]	Fabricating nano-thick film using ALD,[48a,80] Improved wettability with electrolyte[80]

substrate by magnetron sputtering at room temperature, demonstrating its ability for stabilizing Li metal batteries (Figure 5b).[73]

Li_3N stands out as its high ionic conductivity (10^{-3}–10^{-4} S cm^{-1}),[95] enabling fast Li-ion transfer to promote uniform Li deposition. A theoretical simulation demonstrated that the energy barrier for Li-ion migration follows the order $Li_3N < Li_2O < Li_2CO_3 <$ LiF (Figure 5c).[107] This high Li^+ mobility allows Li_3N to be used to enhance the ion conductivity of the artificial interphase. For instance, LiF exhibits a high ion migration barrier, which exacerbates the kinetics of Li-ion diffusion. Wang *et al.* fabricated a LiF/Li_3N-dominated SEI film and found that the synergistic effect of LiF and Li_3N promoted homogeneous and dense Li deposition, exhibiting better electrochemical performance than LiF and Li_3N alone (Figure 5d).[108]

Li_3PO_4 is employed as an artificial interphase material because of its high Young's modulus and high ionic conductivity. Li *et al.* designed a ~200 nm Li_3PO_4 thin SEI layer through the chemical reaction of polyphosphoric acid with Li metal and a native SEI (Figure 5e).[78] The Li_3PO_4 film with a uniform structure exhibits a high Young's modulus (10–11 GPa), high ionic conductivity, and high chemical stability, contributing to a

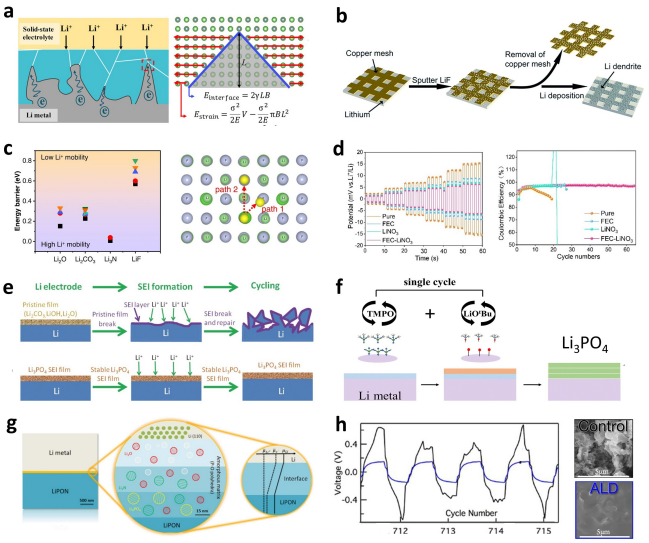

Figure 5. (a) Schematic of interface and strain energy acting on the Li deposition process. Reproduced with permission.[91] Copyright 2018 American Association for the Advancement of Science. (b) Schematic of sputtering LiF to suppress Li dendrite. Reproduced with permission.[73] Copyright 2017 Royal Society of Chemistry. (c) Comparison of diffusion energy for Li^+ diffusion and schematic illustration of two Li^+ diffusion pathways in LiF with energy barrier of 0.18 eV for path 1 and 0.23 eV for path 2. Reproduced with permission.[107] Copyright 2022 Springer Nature. (d) Discharge and charge curves of Li–Li symmetric cell and Coulombic efficiency of Li/Cu cell in pure, FEC, $LiNO_3$, and FEC-$LiNO_3$ electrolytes. Reproduced with permission.[108] Copyright 2024 Royal Society of Chemistry. (e) Schematic of Li_3PO_4 modified Li via chemical reaction. Reproduced with permission.[78] Copyright 2016 Wiley-VCH. (f) Schematic illustration of coating Li_3PO_4 on Li metal by atomic layer deposition.[97] Copyright 2021 Springer Nature. (g) Schematic illustration of Li/LiPON multilayered interphase. Reproduced with permission.[109] Copyright 2020 Elsevier. (h) Discharge and charge curves of a Li–Li symmetric cell show the effects of Al_2O_3 coating. Reproduced with permission.[48a] Copyright 2015 American Chemical Society

stable Li||$LiFePO_4$ cell with 200 cycles. The coated surface film prepared by chemical reactions has the disadvantage of being uncontrollable in terms of thickness and uniformity. Thus, atomic layer deposition (ALD) is further developed to construct a Li_3PO_4 layer on the Li surface, exhibiting a uniform and dense structure with a controllable thickness of 10 nm (Figure 5f).[97]

LiPON, with the chemical formula of $Li_xPO_yN_z$, has been widely used as a solid electrolyte in thin film batteries since its synthesis in the 1990s.[110] It exhibits high mechanical strength (shear modulus 77 GPa[99]) and high ionic conductivity (10^{-6}–10^{-8} S cm^{-1}),[101] making it attractive as an artificial interphase. For example, the high Li-ion conductivity of LiPON can be used to enhance the ionic conductivity of SEI film, as demonstrated by the improvement of pristine LiF conductivity from 1.5×10^{-8} to 1.5×10^{-6} S cm^{-1}.[74] Notably, LiPON is thermodynamically unstable to metallic Li, forming a passivation layer composed of Li_3PO_4, Li_3P, Li_2O and Li_3N on the Li surface.[111] Cryogenic electron microscopy revealed that the passivated layer is a multilayer mosaic SEI with a thickness of 76 nm (Figure 5g).[109] Such passivated layer can stop further chemical reactions between LiPON and Li metal, providing a stable and highly ionically conductive Li/LiPON interphase.

Although pure Al_2O_3 shows a high diffusion barrier for Li ions,[112] an ionically conducting Li–Al–O interphase is generated through the reaction between Al_2O_3 and Li,[113] making it a favorable artificial interphase. Additionally, Al_2O_3 can be directly deposited on the Li surface by ALD at low temperature,[114] achieving a conformal coating with subnanometer thickness control. For example, Kazyak *et al.* employed the ALD technique to successfully modify the Li surface with an ultrathin (~2–3 nm) Al_2O_3 layer, showing steady discharge/charge curves (Figure 5h).[48a] Chen *et al.* further studied the growth mechanism of Al_2O_3 ALD on Li, revealing a faster rate in the initial stage.[80] In addition, they found that the Al_2O_3 film significantly improves the wettability of the electrolyte, promoting uniform and dense SEI formation as well as decreasing electrolyte consumption. Consequently, improved cycling stability can be realized using a tiny amount of electrolyte (5 μL).

However, most inorganic materials suffer from poor flexibility and interfacial contact with coated Li or Cu substrates, making them inefficient for large volume changes and maintaining structural integrity, leading to film cracking during cycling. Thus, when using a single inorganic material, the primary requirement is to fabricate intact films without cracks, which can be achieved by chemical in situ reactions,[78,115] ex-situ coating techniques such as ALD,[80,97] magnetic sputtering,[74,79] molecular-beam epitaxy,[116] and chemical vapor deposition (CVD).[117]. To enhance their affinity with the substrate, composite films are popularly fabricated by incorporating rigid inorganic materials into flexible materials such as carbon materials or organic polymers. For example, Ni *et al.* proposed a composite artificial interphase by the in situ formation of Li_3N and Li_2S on free-standing graphene oxide (GO).[77] The incorporation of Li_3N and Li_2S can considerably enhance Li-ion transfer and mechanical strength, exhibiting a higher Young's modulus (15.8 GPa) than that of GO (7.6 GPa) and the pristine SEI (2.2 GPa).

4.2. Organic Polymer Materials

Organic polymers are prospective candidates for artificial interphase materials because of their remarkable deformation ability to accommodate large volume changes and strong adhesion to the Li substrate. Furthermore, polymers offer the advantage of being customizable in terms of their chemical structure and properties, enabling the design and optimization of specific requirements. However, most polymeric materials exhibit low mechanical strength and poor ionic conductivity. Previous studies have summarized strategies for increasing the ionic conductivity of polymer materials.[9,118] Herein, we mainly focus on improving their mechanical performance.

Appropriate artificial interphase materials for Li anodes should possess both mechanical strength to suppress dendritic Li growth and mechanical flexibility to accommodate large volume changes during cycling. However, it is difficult to fabricate polymeric materials that simultaneously possess mechanical strength and high flexibility. Figure 6 shows the chemical structures of commonly used polymer matrix for

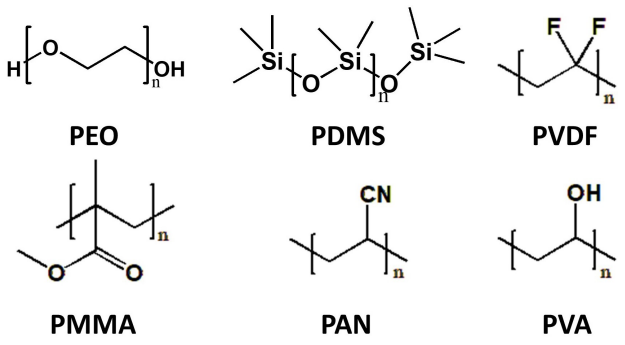

Figure 6. Chemical structure of poly(ethylene oxide) (PEO), poly(dimethylsiloxane) (PDMS), poly(vinylidenefluoride) (PVDF), poly(methyl methacrylate) (PMMA), polyacrylonitrile (PAN), and polyvinyl alcohol (PVA).

preparing artificial interphases in Li metal anodes, including poly(ethylene oxide) (PEO), poly(dimethylsiloxane) (PDMS), poly(vinylidenefluoride) (PVDF), poly(methyl methacrylate) (PMMA), polyacrylonitrile (PAN), and polyvinyl alcohol (PVA).

PEO, with –CH_2–CH_2–O– repeating units, has been widely used as a host polymer matrix for solid polymer electrolytes in LIBs owing to its high dielectric permittivity, high chemical stability, and good chain flexibility.[119] These advantages meet the requirements of SEI, making it an attractive candidate as an artificial interphase material for Li metal anodes.[120] However, its poor mechanical strength renders it inefficient at suppressing Li dendritic growth.[121]

PDMS, owing to its robust –Si–O– bonds, provides high chemical stability and outstanding mechanical flexibility. Zhu *et al.* first applied a PDMS film as an artificial interphase for Li anodes after hydrofluoric acid etching to produce nanopores for Li-ion transportation.[122] Subsequently, PDMS has been widely demonstrated as an effective artificial interphase to stabilize Li metal anodes.[54a,123]

PVDF, with a repeating unit of –CH_2–CF_2–, is a well-known semi-crystalline polymer with several appealing properties, such as high mechanical strength, good binding capacity, high thermal and electrochemical stability, high dielectric constant to promote the dissolution of Li salts, and strong piezoelectric properties for producing large-scale films.[124] Those attractive properties make PVDF and its derivatives widely used as separators, binders, and polymeric electrolytes in Li-ion batteries.[125] Five different crystalline phases have been identified in PVDF, namely α, β, γ, δ, and ε, which are highly dependent on the processing conditions.[126] Among them, β-phase PVDF exhibits the highest dielectric constant and high modulus,[127] making it the preferred choice for use as an artificial protective layer on Li anode. It has been demonstrated that β-phase PVDF coating can be used as an effective artificial layer to inhibit dendritic Li growth.[128] However, PVDF suffers from a low Li^+ migration rate, resulting in low rate performance.[129]

Copolymerization is an effective method for obtaining polymers with high mechanical strength and flexibility. A copolymer is composed of two or more different types of monomer units that exhibit a combination of the properties of each monomer. Soft polymers are generally added to rigid components, whereas hard polymers are commonly incorporated into flexible units. For example, a flexible hexafluoropropylene (HFP) unit was incorporated into thermoplastic PVDF to achieve relatively flexible poly(vinylidene fluoride-hexafluoropropylene) (PVDF-HFP).[130] PMMA was added to decrease the crystallinity of PVDF-HFP, providing high ionic conductivity, high tensile strength, and fraction strain.[131] Styrene-butadiene rubber (SBR) is a copolymer comprising styrene and butadiene monomer units. Balsara *et al.* found that polystyrene-*block*-poly(ethylene oxide) (PS-*b*-PEO) electrolytes exhibits an enhanced ability to suppress Li dendrite growth.[132] This can be attributed to their higher modulus (shear modulus ~0.1 GPa) than that of the PEO homopolymer.

Cross-linking is another effective strategy for improving the mechanical properties of polymeric materials. A crosslinked polymer is also known as a network polymer, in which individual polymer chains are chemically or physically bonded to form a three-dimensional network structure. Compared with uncrosslinked linear or branched polymer chains, the constructed three-dimensional network structure often provides increased resistance to deformation and mechanical strength. In particular, physically crosslinked polymer networks have received increasing attention for realizing mechanical strength and high flexibility.[133] For example, Xiong *et al.* proposed a dynamic gel as a robust artificial interphase through a cross-linking reaction between rigid chitosan (CS) and dibenzaldehyde-terminated telechelic poly(ethylene glycol) (DF-PEG-DF) (Figure 7a).[83] The PEG backbone contributed to flexibility and ionic conductivity, while chitosan with a high Young's modulus of 2.3 GPa was used to enhance mechanical strength. They demonstrated that the obtained gel exhibits a higher mechan-

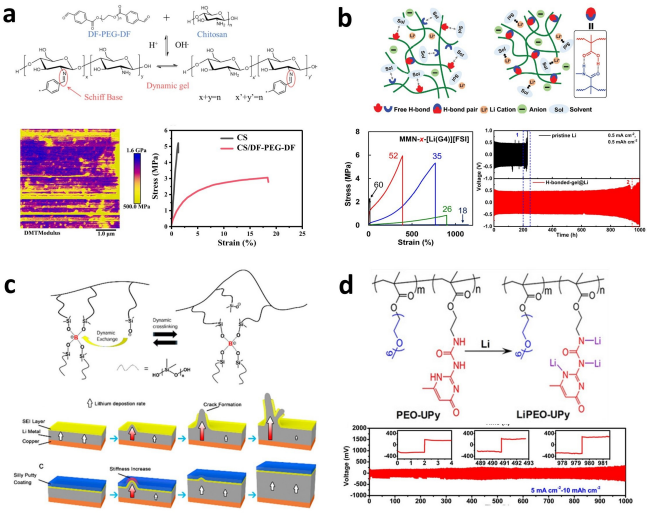

Figure 7. (a) Cross-linked dynamic gel of chitosan and dibenzaldehyde-terminated telechelic poly(ethylene glycol). Reproduced with permission.[83] Copyright 2023 Springer Nature. (b) Hydrogen bonded gel prepared using concentrated electrolyte. Reproduced with permission.[84] Copyright 2023 Wiley-VCH. (c) Viscoelastic Silly putty that shows a solid-liquid behavior. Reproduced with permission.[54a] Copyright 2017, American Chemical Society. (d) Self-healable PEO-Upy polymers. Reproduced with permission.[86] Copyright 2020 Wiley-VCH.

ical strength of 1.0 GP than that of the pristine D-PEG-DF film (164 MPa). We successfully fabricated an extremely tough and flexible gel electrolyte by controlling the competitive hydrogen bonding (H-bonding) interactions between the polymer chains, solvent molecules, Li cations, and counter anions (Figure 7b).[84] Strong interpolymer H-bonds was obtained using a highly concentrated electrolyte. The optimized H-bonded gel exhibits outstanding mechanical properties with a high Young modulus (4.5 MPa), fracture strain (769%), fracture stress (5.3 MPa), and toughness (16 MJ m^{-3}). The obtained results are consistent with those of cutting-edge resilient hydrogels and ion gels. Using it as an artificial interphase for the Li metal anode, the Li–Li symmetric cell can run up to 1000 cycles at a current density of 0.5 mA cm^{-2} with a fixed capacity of 0.5 mAh cm^{-2}.

As a different concept from the realization of both mechanical strength and flexibility, viscoelastic polymers that can adapt to the dynamic changes of the Li metal anode during cycling by utilizing their capability to self-adapt to morphological changes in different regions have attracted considerable attention. Viscoelastic polymers exhibit both viscous (fluid-like) and elastic (solid-like) behaviors under mechanical loads. The "solid–liquid" hybrid feature allows them to transition reversibly between their "liquid" and "solid" states, self-adjusting to adapt to the morphological changes of metallic Li in different states. Silly putty (SP), comprised of polydimethylsiloxane (PDMS) cross-linked by a boron-mediator, is a well-known viscoelastic polymer material.[134] Cui and Bao *et al.* proposed the use of such a "solid–liquid" property as a protective layer for Li metal to adapt to its dynamic surface changes(Figure 7c).[54a] They found that the SP exhibits solid-like behavior to suppress dendritic Li growth at positions where localized deposition of Li metal occurs. Once the local growth rate was restrained, the SP reverted to its liquid-like behavior to accommodate the volume change. Following this work, extensive research has been conducted to study the viscoelastic properties for stabilizing Li metal anodes, demonstrating the effectiveness of viscoelastic materials.[54b,65,135] Based on a 3D coarse-grained molecular simulation model, Kong *et al.* studied the effects of polymer coatings with different mechanical properties on Li dendrite growth.[40] They demonstrated that a viscoelastic polymer is an ideal choice for an artificial layer because of its unique dual advantages of mechanical robustness and adaptability.

Similarly, self-healing materials have the ability to autonomously repair physical damage.[136] This feature is highly desirable for achieving stable Li metal anodes, especially considering that the SEI inevitably experiences mechanical damage during long-term cycling. Employing a reversible cross-linking point is a common way to obtain self-healing ability.[137] For example, a fast self-healing and single-ion conductive polymer was designed as an artificial interphase for Li metal anodes through dynamic covalent crosslinking of PDMS.[138] The self-healing capability of the material is stemmed from dynamic Al–O bonds at crosslinking centers, while its Li-ion selectivity is attributed to the presence of negatively charged $Al(OR)_4^-$ group. After further optimization using SiO_2 nanoparticles to improve the mechanical properties, a stable Li metal anode is achieved, running for up to 1340 h at 0.5 mA cm^{-2} of 1.0 mAh cm^{-2}. In addition, noncovalent interactions have also been demonstrated as a promising strategy to achieve self-healing capabilities.[139] 2-Ureido-4-pyrimidone (UPy), with quadruple hydrogen bonding, has been widely demonstrated as an effective monomer for fabricating self-healing polymers.[140] Wang *et al.*[86] fabricated self-healing PEO-UPy polymers (Figure 7d). Using it as an artificial interphase for Li anodes, long cycle life of over 1000 h is obtained at 5 mA cm^{-2} with an ultrahigh areal capacity of 10 mAh cm^{-2}.

4.3. Inorganic/Organic Hybrid Materials

Inorganic/organic hybrid materials consisting of inorganic and organic polymers have garnered increasing attention owing to their ability to integrate the advantages of both inorganic and organic materials.[142] In such hybrid materials, the polymeric matrix provides mechanical flexibility to adapt to volumetric changes and maintain structural integrity during Li cycling. The inorganic phase provides mechanical stiffness, which suppresses Li dendrite generation. In addition, when Li-conducting inorganic particles are employed, Li-ion conductivity may be further enhanced by the introduction of an additional conducting pathway. However, it is challenging to ensure a good chemical and mechanical compatibility between the inorganic and organic phases. Incompatibility can lead to phase separation or uneven distribution, reducing the effectiveness of the SEI.

To solve this problem, Cui *et al.* proposed a rational design of a composite artificial interphase with inorganic Cu_3N nanoparticles joined together by SBR polymeric binder (Figure 8a), which simultaneously exhibits enhanced ionic conductivity, good flexibility, and enhanced mechanical stability with a high elastic modulus of 0.81 GPa.[61b] Cu_3N nanoparticles react with metallic Li to form Li_3N covered on the deposited Li, promoting fast Li transport. Huang *et al.* found that Young's modulus of the soft PVDF-HFP film is significantly enhanced from 0.8 to 6.72 GPa after adding rigid LiF particles.[87] Consequently, a dendrite-free Li metal anode with high Coulombic efficiency and long cycling performance is achieved. To further strengthen the connection between the inorganic phase and polymer matrix, Cao *et al.* fabricated poly(ethylene glycol) diacrylate

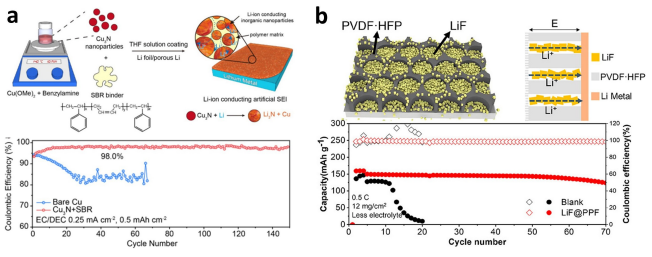

Figure 8. (a) Schematic illustration of the fabrication of Cu_3N/SBR composite artificial interphase and cell performance of Li–Cu cell. Reproduced with permission.[61b] Copyright 2017 Wiley-VCH. (b) Schematic illustration of LiF nanoparticles confined within hierarchically porous channels and the cell performance of Li||$LiFePO_4$ full cell. Reproduced with permission.[141] Copyright 2023 American Chemical Society.

(PEGDA)/lithium difluoro(oxalato)borate $LiBF_2(C_2O_4)$(LiDFOB) composite SEI film by in-situ polymerization of precursor.[143] Yu and coworkers fabricated a PVDF-HFP matrix with hierarchically porous channels to spatially confine LiF nanoparticles (LiF@PVDF-HFP) (Figure 8b).[141] The fabricated LiF@ PVDF-HFP exhibits a high Young's modulus of 5.2 GPa and promotes uniform Li-ion transport.

In summary, we have reviewed three types of materials as artificial interface layers: inorganic, organic polymer, and inorganic/organic hybrid materials. Each type of material offers distinct advantages and disadvantages when used as an artificial interphase in Li metal anodes, as detailed in Table 3. Inorganic materials provide good mechanical robustness, high ionic conductivity, and high chemical and thermal stability. However, they often suffer from poor flexibility and brittleness. Organic polymers stand out due to their high flexibility, strong adhesiveness to Li, and facile modulation of chemical structure and resultant mechanical properties. Nevertheless, they generally exhibit lower mechanical strength, making them less effective in preventing dendritic Li growth. Inorganic/organic hybrid materials offer balanced mechanical strength and flexibility, as well as improved ionic conductivity by combining the benefits of both inorganic and organic components. However, achieving seamless integration and uniform distribution of these components remains challenging.

5. Summary and Outlook

In conclusion, we summarized the fabrication strategy for effective artificial interphase materials for Li metal anodes from the perspective of mechanical properties by discussing the underlying mechanism of SEI fracture, the critical requirements for the mechanical properties of SEI layers, mechanical measurements to quantify mechanical properties, and recent progress in fabricating mechanically stable artificial interphase materials for Li metal anodes.

5.1. Fundamental Mechanism underlying SEI Fracture

Theoretical studies and in-situ observations can help understand the SEI fracture mechanism and provide guidance for reasonably designing artificial interphases. Because it is very difficult to simulate and monitor mechanical deformation in practical cell systems, most theoretical studies have been conducted on simplified models such as linear elastic deformation or elastic–plastic deformation. However, recent studies have suggested that more complex deformations should be considered to understand the SEI fracture mechanism during Li growth kinetics. For experimental measurements, ETEM is a promising new technique for the real-time monitoring of mechanical stress within Li metal during the electrodeposition process. However, external pressure can alter the direction of Li growth, thereby changing the stress and morphology of the deposited Li. Thus, there is an urgent need to develop an in-situ observation method that can simulate practical cell systems, particularly under certain external pressures.

5.2. Mechanical Requirements and Evaluation of SEI

The quantification of mechanical parameters can provide better guidance for designing artificial interphases. Obtaining accurate and reliable data is crucial for measuring mechanical properties. However, the test results are influenced by various factors, such as sample fabrication, substrate, and measurement conditions. To facilitate communication among scientists and enable the comparison of different test data, it is recommended to provide detailed sample preparation information, establish standardized testing conditions, and present data analysis procedures. Furthermore, estimating the target values of the mechanical properties required for artificial interphases in practical systems is challenging, as they are influenced by various other factors, such as ionic transport properties, structural uniformity, surface roughness, coating thickness, and applied current or potential. To overcome these issues, it is essential to develop experimental methods and multiscale simulations that can observe and predict the stress-strain distributions in practical batteries.

5.3. Promising Artificial Interphase Materials

Various inorganic and organic polymers have been used as artificial interphase materials. Each material has its advantages and disadvantages, including poor flexibility and low mechan-

Table 3. Comparison of the advantages and disadvantages of inorganic, organic polymer, and inorganic/organic hybrid materials.

Type	Advantages	Disadvantages
Inorganic materials	Good mechanical robustness to suppress dendrite growth High ionic conductivity High chemical and thermal stability	Poor flexibility Brittleness Poor affinity with substrates
Organic polymer	High flexibility to accommodate volume changes Strong adhesiveness to Li Modifiable chemical structure and mechanical properties	Low mechanical strength Poor ionic conductivity Poor chemical stability in electrolyte
Inorganic/organic hybrid materials	Balanced mechanical strength and flexibility High ionic conductivity by combing the strengths of both inorganic and organic materials	Incompatibility between inorganic and organic phases Interface issues between different materials

ical strength. The introduction of precisely tuned cross-linking networks and the fabrication of inorganic/organic hybrid materials are promising approaches for achieving both high mechanical strength and flexibility. In addition, other intelligent concepts, such as self-adaptable viscoelastic polymers and self-healing materials, may be effective in protecting Li metal anodes.

In addition to mechanical performance, it is necessary to consider other important factors, such as ion/electron transport properties, (electro)chemical stability, structural uniformity, and adhesion to the substrate. To optimize artificial interphases effectively, advanced computational techniques such as artificial intelligence (AI), machine learning, and high-throughput computing hold significant promise. AI algorithms can analyze vast datasets to identify promising materials as artificial interphases for Li metal anodes. Machine learning can predict the properties and performances of novel materials prior to experimental validation, thereby reducing both time and cost. High-throughput computing techniques can rapidly screen numerous material combinations and configurations to identify candidates with superior mechanical stability, ionic conductivity and other desirable properties. These computational technologies offer a comprehensive approach to streamline the discovery and optimization processes, and ultimately lead to the design of more durable and efficient interphases for Li metal anodes.

Acknowledgements

This study was supported by grants from the Japan Science and Technology Agency COI-NEXT program (Grant No. JPMJPF2016), the Green Technologies of Excellence (GteX) program (Grant No. JPMJGX23S3), and JSPS KAKENHI (Grant No. 23K26409).

Conflict of Interests

The authors declare no conflict of interest.

Data Availability Statement

The data that support the findings of this study are available from the corresponding author upon reasonable request.

Keywords: solid electrolyte interphase (SEI) · artificial interphase · Li anode · Li dendrite · mechanical properties

[1] a) J. B. Goodenough, Y. Kim, *Chem. Mater.* **2009**, *22*, 587–603; b) H. Zhou, F. Xin, B. Pei, M. S. Whittingham, *ACS Energy Lett.* **2019**, *4*, 1902–1906.
[2] D. Lin, Y. Liu, Y. Cui, *Nat. Nanotechnol.* **2017**, *12*, 194–206.
[3] X. Hong, J. Mei, L. Wen, Y. Tong, A. J. Vasileff, L. Wang, J. Liang, Z. Sun, S. X. Dou, *Adv. Mater.* **2019**, *31*, 1802822.
[4] a) C. Fang, X. Wang, Y. S. Meng, *Trends Chem.* **2019**, *1*, 152–158; b) X. B. Cheng, R. Zhang, C. Z. Zhao, Q. Zhang, *Chem. Rev.* **2017**, *117*, 10403–10473.
[5] a) H. Wu, H. Jia, C. Wang, J. Zhang, W. Xu, *Adv. Energy Mater.* **2020**, *11*, 2003092; b) Y. Xu, K. Dong, Y. Jie, P. Adelhelm, Y. Chen, L. Xu, P. Yu, J. Kim, Z. Kochovski, Z. Yu, W. Li, J. LeBeau, Y. Shao Horn, R. Cao, S. Jiao, T. Cheng, I. Manke, Y. Lu, *Adv. Energy Mater.* **2022**, *12*, 2200398.
[6] a) B. Horstmann, J. Shi, R. Amine, M. Werres, X. He, H. Jia, F. Hausen, I. Cekic Laskovic, S. Wiemers Meyer, J. Lopez, D. Galvez Aranda, F. Baakes, D. Bresser, C. C. Su, Y. Xu, W. Xu, P. Jakes, R. A. Eichel, E. Figgemeier, U. Krewer, J. M. Seminario, P. B. Balbuena, C. Wang, S. Passerini, Y. Shao Horn, M. Winter, K. Amine, R. Kostecki, A. Latz, *Energy Environ. Sci.* **2021**, *14*, 5289–5314; b) X. B. Cheng, R. Zhang, C. Z. Zhao, F. Wei, J. G. Zhang, Q. Zhang, *Adv. Sci.* **2016**, *3*, 1500213.
[7] R. Xu, X. Cheng, C. Yan, X. Zhang, Y. Xiao, C. Zhao, J. Huang, Q. Zhang, *Matter.* **2019**, *1*, 317–344.
[8] Z. Yu, Y. Cui, Z. Bao, *Cell Rep.* **2020**, *1*, 100119.
[9] S. Gao, F. Sun, N. Liu, H. Yang, P. Cao, *Mater. Today* **2020**, *40*, 140–159.
[10] B. Jagger, M. Pasta, *Joule* **2023**, *7*, 2228–2244.
[11] a) P. Barai, K. Higa, V. Srinivasan, *J. Electrochem. Soc.* **2016**, *164*, A180–A191; b) J. D. McBrayer, C. A. Apblett, K. L. Harrison, K. R. Fenton, S. D. Minteer, *Nanotechnology* **2021**, *32*, 1–25.
[12] a) P. Liang, G. Shao, H. Wang, C. Wang, *ACS Appl. Energ. Mater.* **2021**, *4*, 3993–4001; b) M. Diaz, A. Kushima, *J. Electrochem. Soc.* **2021**, *168*, 020535.
[13] Y. S. Cohen, Y. Cohen, D. Aurbach, *J. Phys. Chem. B.* **2000**, *104*, 12282–12291.
[14] D. Aurbach, *J. Power Sources* **2000**, *89*, 206–218.
[15] E. Peled, S. Menkin, *J. Electrochem. Soc.* **2017**, *164*, A1703–A1721.
[16] Y. Li, Y. Li, A. Pei, K. Yan, Y. Sun, C. Wu, L. Joubert, R. Chin, A. L. Koh, Y. Yu, *Science* **2017**, *358*, 506–510.
[17] E. Peled, *J. Electrochem. Soc.* **1979**, *126*, 2047–2053.
[18] M. Winter, *Zeitschrift für Phys. Chemie* **2009**, *223*, 1395–1406.
[19] a) D. Aurbach, I. Weissman, A. Schechter, H. Cohen, *Langmuir* **1996**, *12*, 3991–4007; b) D. Aurbach, M. Daroux, P. Faguy, E. Yeager, *J. Electrochem. Soc.* **1987**, *134*, 1611–1622; c) D. Aurbach, Y. Gofer, J. Langzam, *J. Electrochem. Soc.* **1989**, *136*, 3198–3207; d) D. Aurbach, Y. Cohen, *J. Electrochem. Soc.* **1996**, *143*, 3525–3534.
[20] A. Schechter, D. Aurbach, H. Cohen, *Langmuir* **1999**, *15*, 3334–3342.
[21] a) K. Kanamura, H. Takezawa, S. Shiraishi, Z. i. Takehara, *J. Electrochem. Soc.* **1997**, *144*, 1900–1908; b) K. Kanamura, S. Shiraishi, H. Tamura, Z. i. Takehara, *J. Electrochem. Soc.* **1994**, *141*, 2379–2387; c) Y. Liu, Z. Ju, B. Zhang, Y. Wang, J. Nai, T. Liu, X. Tao, *Acc. Chem. Res.* **2021**, *54*, 2088–2099.
[22] H. Shin, J. Park, S. Han, A. M. Sastry, W. Lu, *J. Power Sources* **2015**, *277*, 169–179.
[23] B. Wolff, F. Hausen, *J. Electrochem. Soc.* **2023**, *170*, 010534.
[24] R. L. Sacci, J. M. Black, N. Balke, N. J. Dudney, K. L. More, R. R. Unocic, *Nano Lett.* **2015**, *15*, 2011–2018.
[25] K. Nishikawa, K. Shinoda, *J. Electrochem. Soc.* **2022**, *169*, 102507.
[26] I. Yoon, S. Jurng, D. P. Abraham, B. L. Lucht, P. R. Guduru, *Energy Storage Mater.* **2020**, *25*, 296–304.
[27] A. Kushima, K. P. So, C. Su, P. Bai, N. Kuriyama, T. Maebashi, Y. Fujiwara, M. Z. Bazant, J. Li, *Nano Energy* **2017**, *32*, 271–279.
[28] L. Zhang, T. Yang, C. Du, Q. Liu, Y. Tang, J. Zhao, B. Wang, T. Chen, Y. Sun, P. Jia, H. Li, L. Geng, J. Chen, H. Ye, Z. Wang, Y. Li, H. Sun, X. Li, Q. Dai, Y. Tang, Q. Peng, T. Shen, S. Zhang, T. Zhu, J. Huang, *Nat. Nanotechnol.* **2020**, *15*, 94–98.
[29] A. Kushima, K. P. So, C. Su, P. Bai, N. Kuriyama, T. Maebashi, Y. Fujiwara, M. Z. Bazant, J. Li, *Nano Energy* **2017**, *32*, 271–279.
[30] a) A. Jana, S. I. Woo, K. S. N. Vikrant, R. E. García, *Energy Environ. Sci.* **2019**, *12*, 3595–3607; b) G. Yoon, S. Moon, G. Ceder, K. Kang, *Chem. Mater.* **2018**, *30*, 6769–6776; c) L. T. Gao, P. Huang, Z.-S. Guo, *J. Electrochem. Soc.* **2022**, *169*, 060522.
[31] F. Shi, A. Pei, D. T. Boyle, J. Xie, X. Yu, X. Zhang, Y. Cui, *Proc. Natl. Acad. Sci. USA* **2018**, *115*, 8529–8534.
[32] a) K. Nishikawa, T. Mori, T. Nishida, Y. Fukunaka, M. Rosso, T. Homma, *J. Electrochem. Soc.* **2010**, *157*, A1212; b) K. Nishikawa, H. Naito, M. Kawase, T. Nishida, *ECS Trans.* **2012**, *41*, 3–10.
[33] W. Wang, Y. Gu, J. Wang, Z. Chen, X. Yin, Q. Wu, J. Yan, B. Mao, *J. Electrochem. Soc.* **2022**, *169*, 020563.
[34] a) H. Sun, Q. Liu, J. Chen, Y. Li, H. Ye, J. Zhao, L. Geng, Q. Dai, T. Yang, H. Li, Z. Wang, L. Zhang, Y. Tang, J. Huang, *ACS Nano* **2021**, *15*, 19070–19079; b) Y. He, X. Ren, Y. Xu, M. H. Engelhard, X. Li, J. Xiao, J. Liu, J. G. Zhang, W. Xu, C. Wang, *Nat. Nanotechnol.* **2019**, *14*, 1042–1047.
[35] R. P. Schultz, *Fermi National Accelerator Lab.* **2002**, 1–6.
[36] C. Xu, Z. Ahmad, A. Aryanfar, V. Viswanathan, J. R. Greer, *Proc. Natl. Acad. Sci. USA* **2017**, *114*, 57–61.

[37] C. Monroe, J. Newman, *J. Electrochem. Soc.* **2005**, *152*, A396–A406.
[38] P. Barai, K. Higa, V. Srinivasan, *Phys. Chem. Chem. Phys.* **2017**, *19*, 20493–20505.
[39] Y. Gao, X. Du, Z. Hou, X. Shen, Y. Mai, J. Tarascon, B. Zhang, *Joule* **2021**, *5*, 1860–1872.
[40] X. Kong, P. E. Rudnicki, S. Choudhury, Z. Bao, J. Qin, *Adv. Funct. Mater.* **2020**, *30*, 1910138.
[41] X. Shen, R. Zhang, X. Chen, X. Cheng, X. Li, Q. Zhang, *Adv. Energy Mater.* **2020**, *10*, 1903645.
[42] Y. Liu, X. Xu, O. O. Kapitanova, P. V. Evdokimov, Z. Song, A. Matic, S. Xiong, *Adv. Energy Mater.* **2022**, *12*, 2103589.
[43] a) C. R. Pals, J. Newman, *J. Electrochem. Soc.* **1995**, *142*, 3274; b) C. R. Pals, J. Newman, *J. Electrochem. Soc.* **1995**, *142*, 3282.
[44] a) M. Doyle, T. F. Fuller, J. Newman, *J. Electrochem. Soc.* **1993**, *140*, 1526; b) T. F. Fuller, M. Doyle, J. Newman, *J. Electrochem. Soc.* **1994**, *141*, 1.
[45] C. Monroe, J. Newman, *J. Electrochem. Soc.* **2003**, *150*, A1377.
[46] C. Monroe, J. Newman, *J. Electrochem. Soc.* **2004**, *151*, A880–A888.
[47] K. J. Harry, K. Higa, V. Srinivasan, N. P. Balsara, *J. Electrochem. Soc.* **2016**, *163*, A2216–A2226.
[48] a) E. Kazyak, K. N. Wood, N. P. Dasgupta, *Chem. Mater.* **2015**, *27*, 6457–6462; b) D. Zhou, R. Liu, Y. B. He, F. Li, M. Liu, B. Li, Q. H. Yang, Q. Cai, F. Kang, *Adv. Energy Mater.* **2016**, *6*, 1502214.
[49] a) Y. Liu, Y. Tzeng, D. Lin, A. Pei, H. Lu, N. A. Melosh, Z.-X. Shen, S. Chu, Y. Cui, *Joule* **2018**, *2*, 1595–1609; b) G. Zheng, S. W. Lee, Z. Liang, H. W. Lee, K. Yan, H. Yao, H. Wang, W. Li, S. Chu, Y. Cui, *Nat. Nanotechnol.* **2014**, *9*, 618–623.
[50] A. Ferrese, J. Newman, *J. Electrochem. Soc.* **2014**, *161*, A1350.
[51] F. Hao, W. Wang, P. P. Mukherjee, *Phys. Rev. Appl.* **2019**, *11*, 034038.
[52] K. Liu, P. Bai, M. Z. Bazant, C. A. Wang, J. Li, *J. Mater. Chem. A.* **2017**, *5*, 4300–4307.
[53] D. R. Ely, R. E. García, *J. Electrochem. Soc.* **2013**, *160*, A662–A670.
[54] a) K. Liu, A. Pei, H. R. Lee, B. Kong, N. Liu, D. Lin, Y. Liu, C. Liu, P. C. Hsu, Z. Bao, Y. Cui, *J. Am. Chem. Soc.* **2017**, *139*, 4815–4820; b) Q. Ma, X. Zeng, J. Yue, Y. X. Yin, T. Zuo, J. Liang, Q. Deng, X. Wu, Y. Guo, *Adv. Energy Mater.* **2019**, *9*, 1803854.
[55] a) J. Lopez, A. Pei, J. Y. Oh, G. N. Wang, Y. Cui, Z. Bao, *J. Am. Chem. Soc.* **2018**, *140*, 11735–11744; b) P. Barai, K. Higa, V. Srinivasan, *J. Electrochem. Soc.* **2018**, *165*, A2654–A2668.
[56] S. Correa, A. K. Grosskopf, H. Lopez Hernandez, D. Chan, A. C. Yu, L. M. Stapleton, E. A. Appel, *Chem. Rev.* **2021**, *121*, 11385–11457.
[57] G. Kada, F. Kienberger, P. Hinterdorfer, *Nano Today* **2008**, *3*, 12–19.
[58] L. Ladani, E. Harvey, S. Choudhury, C. Taylor, *Exp. Mech.* **2013**, *53*, 1299–1309.
[59] a) Y. Liu, R. Hu, D. Zhang, J. Liu, F. Liu, J. Cui, Z. Lin, J. Wu, M. Zhu, *Adv. Mater.* **2021**, *33*, 2004711; b) N. W. Li, Y. Shi, Y. X. Yin, X. X. Zeng, J. Y. Li, C. J. Li, L. J. Wan, R. Wen, Y. G. Guo, *Angew. Chem. Int. Ed.* **2018**, *57*, 1505–1509.
[60] S. Lang, Z. Shen, X. Hu, Y. Shi, Y. Guo, F. Jia, F. Wang, R. Wen, L. Wan, *Nano Energy* **2020**, *75*, 104967.
[61] a) Y. Kamikawa, K. Amezawa, K. Terada, *J. Phys. Chem. C.* **2020**, *124*, 22488–22495; b) Y. Liu, D. Lin, P. Y. Yuen, K. Liu, J. Xie, R. H. Dauskardt, Y. Cui, *Adv. Mater.* **2017**, *29*, 1605531.
[62] A. Hannon, P. Tiernan, *J. Mater. Process. Technol.* **2008**, *198*, 1–13.
[63] M. Bazli, M. Abolfazli, *Polymer* **2020**, *12*, 2600.
[64] A. Mei, H. Kindlund, E. Broitman, L. Hultman, I. Petrov, J. E. Greene, D. Sangiovanni, *Acta Mater.* **2020**, *192*, 78–88.
[65] S. Wei, Z. Cheng, P. Nath, M. D. Tikekar, G. Li, L. A. Archer, *Sci. Adv.* **2018**, *4*, eaao6243.
[66] a) A. N. Patel, C. Kranz, *Annu. Rev. Anal. Chem.* **2018**, *11*, 329–350; b) C. Franz, P. Puech, *Cellular and Molecular Bioengineering* **2008**, *1*, 289–300.
[67] C. A. Clifford, M. P. Seah, *Appl. Surf. Sci.* **2005**, *252*, 1915–1933.
[68] a) E. T. Herruzo, A. P. Perrino, R. Garcia, *Nat. Commun.* **2014**, *5*, 3126; b) R. García, *Amplitude modulation atomic force microscopy*, John Wiley & Sons, **2011**.
[69] B. Pittenger, N. Erina, C. Su, in *Nanomechanical analysis of high performance materials*, Springer, **2013**, pp. 31–51.
[70] a) G. A. Matei, E. J. Thoreson, J. R. Pratt, D. B. Newell, N. A. Burnham, *Rev. Sci. Instrum.* **2006**, *77*, 1–6; b) K. D. Bouzakis, N. Michailidis, S. Hadjiyiannis, G. Skordaris, G. Erkens, *Mater. Charact.* **2002**, *49*, 149–156; c) L. S. Moura, G. D. Vittoria, A. H. G. Gabriel, E. B. Fonseca, L. P. Gabriel, T. J. Webster, É. S. N. Lopes, *J. Mater. Sci.* **2020**, *55*, 9578–9596; d) R. H. Alasfar, S. Ahzi, N. Barth, V. Kochkodan, M. Khraisheh, M. Koc, *Polymer* **2022**, *14*, 360.
[71] R. Saha, W. D. Nix, *Acta Mater.* **2002**, *50*, 23–38.
[72] a) R. Rodriguez, I. Gutierrez, *Mater. Sci. Eng. A.* **2003**, *361*, 377–384; b) D. Krumwiede, T. Yamamoto, T. A. Saleh, S. A. Maloy, G. Odette, P. Hosemann, *J. Nucl. Mater.* **2018**, *504*, 135–143.
[73] L. Fan, H. L. Zhuang, L. Gao, Y. Lu, L. A. Archer, *J. Mater. Chem. A.* **2017**, *5*, 3483–3492.
[74] J. Sun, S. Zhang, J. Li, B. Xie, J. Ma, S. Dong, G. Cui, *Adv. Mater.* **2023**, *35*, 2209404.
[75] A. Hu, W. Chen, X. Du, Y. Hu, T. Lei, H. Wang, L. Xue, Y. Li, H. Sun, Y. Yan, J. Long, C. Shu, J. Zhu, B. Li, X. Wang, J. Xiong, *Energy Environ. Sci.* **2021**, *14*, 4115–4124.
[76] Y. Li, Y. Sun, A. Pei, K. Chen, A. Vailionis, Y. Li, G. Zheng, J. Sun, Y. Cui, *ACS Cent. Sci.* **2018**, *4*, 97–104.
[77] S. Ni, M. Zhang, C. Li, R. Gao, J. Sheng, X. Wu, G. Zhou, *Adv. Mater.* **2023**, *35*, e2209028.
[78] N. W. Li, Y. X. Yin, C. P. Yang, Y. G. Guo, *Adv. Mater.* **2016**, *28*, 1853–1858.
[79] L. Wang, Q. Wang, W. Jia, S. Chen, P. Gao, J. Li, *J. Power Sources* **2017**, *342*, 175–182.
[80] L. Chen, J. G. Connell, A. Nie, Z. Huang, K. R. Zavadil, K. C. Klavetter, Y. Yuan, S. Sharifi Asl, R. Shahbazian-Yassar, J. A. Libera, A. U. Mane, J. W. Elam, *J. Mater. Chem. A.* **2017**, *5*, 12297–12309.
[81] Y. Gao, Y. Zhao, Y. C. Li, Q. Huang, T. E. Mallouk, D. Wang, *J. Am. Chem. Soc.* **2017**, *139*, 15288–15291.
[82] S. Li, J. Huang, Y. Cui, S. Liu, Z. Chen, W. Huang, C. Li, R. Liu, R. Fu, D. Wu, *Nat. Nanotechnol.* **2022**, *17*, 613–621.
[83] C. Chen, J. Zhang, B. Hu, Q. Liang, X. Xiong, *Nat. Commun.* **2023**, *14*, 4018.
[84] R. Tamate, Y. Peng, Y. Kamiyama, K. Nishikawa, *Adv. Mater.* **2023**, *35*, 2211679.
[85] R. M. Gao, H. Yang, C. Y. Wang, H. Ye, F. F. Cao, Z. P. Guo, *Angew. Chem. Int. Ed.* **2021**, *60*, 25508–25513.
[86] G. Wang, C. Chen, Y. Chen, X. Kang, C. Yang, F. Wang, Y. Liu, X. Xiong, *Angew. Chem. Int. Ed.* **2020**, *59*, 2055–2060.
[87] R. Xu, X. Zhang, X. Cheng, H. Peng, C. Zhao, C. Yan, J. Huang, *Adv. Funct. Mater.* **2018**, *28*, 1705838.
[88] Z. Yu, S. Seo, J. Song, Z. Zhang, S. T. Oyakhire, Y. Wang, R. Xu, H. Gong, S. Zhang, Y. Zheng, Y. Tsao, L. Mondonico, E. G. Lomeli, X. Wang, W. Kim, K. Ryu, Z. Bao, *Adv. Energy Mater.* **2022**, *12*, 2201025.
[89] X. Sun, S. Yang, T. Zhang, Y. Shi, L. Dong, G. Ai, D. Li, W. Mao, *Nanoscale* **2022**, *14*, 5033–5043.
[90] X. Liu, J. Liu, T. Qian, H. Chen, C. Yan, *Adv. Mater.* **2020**, *32*, 1902724.
[91] X. Fan, X. Ji, F. Han, J. Yue, J. Chen, L. Chen, T. Deng, J. Jiang, C. Wang, *Sci. Adv.* **2018**, *4*, eaau9245.
[92] Y. Lin, Z. Liu, K. Leung, L. Chen, P. Lu, Y. Qi, *J. Power Sources* **2016**, *309*, 221–230.
[93] Y. Zhu, X. He, Y. Mo, *ACS Appl. Mater. Interfaces* **2015**, *7*, 23685–23693.
[94] F. N. Islam, A. K. M. A. Islam, M. A. Hossain, *J. Sci. Res.* **2009**, *1*, 182–191.
[95] a) U. Alpen, *J. Solid State Chem.* **1979**, *29*, 379–392; b) T. Lapp, S. Skaarup, A. Hooper, *Solid State Ionics* **1983**, *11*, 97–103.
[96] Y. Zhu, X. He, Y. Mo, *Adv. Sci.* **2017**, *4*, 1600517.
[97] J. Niu, M. Wang, T. Cao, X. Cheng, R. Wu, H. Liu, Y. Zhang, X. Liu, *Ionics* **2021**, *27*, 2445–2454.
[98] D. Cheng, T. Wynn, B. Lu, M. Marple, B. Han, R. Shimizu, B. Sreenarayanan, J. Bickel, P. Hosemann, Y. Yang, H. Nguyen, W. Li, G. Zhu, M. Zhang, Y. S. Meng, *Nat. Nanotechnol.* **2023**, *18*, 1448–1455.
[99] E. G. Herbert, W. E. Tenhaeff, N. J. Dudney, G. M. Pharr, *Thin Solid Films* **2011**, *520*, 413–418.
[100] F. Xu, L. Belliard, D. Fournier, E. Charron, J. Y. Duquesne, S. Martin, C. Secouard, B. Perrin, *Thin Solid Films* **2013**, *548*, 366–370.
[101] H. T. Kim, T. Mun, C. Park, S. W. Jin, H. Y. Park, *J. Power Sources* **2013**, *244*, 641–645.
[102] S. Ruppi, A. Larsson, A. Flink, *Thin Solid Films* **2008**, *516*, 5959–5966.
[103] a) G. Ma, Z. Wen, M. Wu, C. Shen, Q. Wang, J. Jin, X. Wu, *Chem. Commun.* **2014**, *50*, 14209–14212; b) Y. J. Zhang, W. Wang, H. Tang, W. Q. Bai, X. Ge, X. L. Wang, C. D. Gu, J. P. Tu, *J. Power Sources* **2015**, *277*, 304–311.
[104] a) J. Ko, D. H. Cho, D. J. Kim, Y. S. Yoon, *J. Alloys Compd.* **2020**, *845*, 156280; b) C. Wang, G. Bai, Y. Yang, X. Liu, H. Shao, *Nano Res.* **2018**, *12*, 217–223.
[105] a) Y. Peng, K. Nishikawa, K. Kanamura, *J. Electrochem. Soc.* **2022**, *169*, 060548; b) Y. Liu, X. Tao, Y. Wang, C. Jiang, C. Ma, O. Sheng, G. Lu, X. W. Lou, *Science* **2022**, *375*, 739–745; c) T. Li, X. Zhang, P. Shi, Q. Zhang, *Joule* **2019**, *3*, 2647–2661; d) Z. Cheng, Y. Chen, L. Shi, M. Wu, Z.

Wen, *ACS Appl. Mater. Interfaces* **2023**, *15*, 10585–10592; e) D. Aurbach, E. Markevich, G. Salitra, *J. Am. Chem. Soc.* **2021**, *143*, 21161–21176.
[106] M. De Jong, W. Chen, T. Angsten, A. Jain, R. Notestine, A. Gamst, M. Sluiter, C. Krishna Ande, S. Van Der Zwaag, J. J. Plata, *Sci. Data* **2015**, *2*, 1–13.
[107] S. Zhang, R. Li, N. Hu, T. Deng, S. Weng, Z. Wu, D. Lu, H. Zhang, J. Zhang, X. Wang, L. Chen, L. Fan, X. Fan, *Nat. Commun.* **2022**, *13*, 5431.
[108] S. Wang, J. Zhang, L. Zhang, X. Li, R. Zhao, Y. Liu, Z. Wang, X. Lu, Y. Xin, H. Tian, F. Kang, B. Li, *J. Mater. Chem. A.* **2024**, 5815–5823.
[109] D. Cheng, T. A. Wynn, X. Wang, S. Wang, M. Zhang, R. Shimizu, S. Bai, H. Nguyen, C. Fang, M. Kim, W. Li, B. Lu, S. J. Kim, Y. S. Meng, *Joule* **2020**, *4*, 2484–2500.
[110] a) J. Bates, N. Dudney, G. Gruzalski, R. Zuhr, A. Choudhury, C. Luck, J. Robertson, *Solid State Ionics* **1992**, *53*, 647–654; b) J. Bates, N. Dudney, G. Gruzalski, R. Zuhr, A. Choudhury, C. Luck, J. Robertson, *J. Power Sources* **1993**, *43*, 103–110.
[111] A. Schwöbel, R. Hausbrand, W. Jaegermann, *Solid State Ionics* **2015**, *273*, 51–54.
[112] S. Hao, C. Wolverton, *J. Phys. Chem. C.* **2013**, *117*, 8009–8013.
[113] a) J. S. Park, X. Meng, J. W. Elam, S. Hao, C. Wolverton, C. Kim, J. Cabana, *Chem. Mater.* **2014**, *26*, 3128–3134; b) J. A. Nguyen, A. Becker, K. Kanhaiya, H. Heinz, A. W. Weimer, *ACS Appl. Mater. Interfaces* **2024**, *16*, 1861–1875.
[114] M. Groner, F. Fabreguette, J. Elam, S. George, *Chem. Mater.* **2004**, *16*, 639–645.
[115] a) C. Sun, A. Lin, W. Li, J. Jin, Y. Sun, J. Yang, Z. Wen, *Adv. Energy Mater.* **2019**, *10*, 1902989; b) Z. Cheng, M. Wu, J. Jin, Y. Lu, Z. Wen, *Electrochim. Acta* **2023**, *464*, 142880; c) M. Cai, J. Jin, T. Xiu, Z. Song, M. E. Badding, Z. Wen, *Energy Storage Mater.* **2022**, *47*, 61–69; d) M. Wu, Z. Wen, J. Jin, B. V. Chowdari, *ACS Appl. Mater. Interfaces.* **2016**, *8*, 16386–16395.
[116] T. Chen, F. Meng, Z. Zhang, J. Liang, Y. Hu, W. Kong, X. L. Zhang, Z. Jin, *Nano Energy* **2020**, *76*, 105068.
[117] a) F. Liu, Q. Xiao, H. Wu, L. Shen, D. Xu, M. Cai, Y. Lu, *Adv. Energy Mater.* **2017**, *8*, 1701744; b) A. A. Assegie, C. C. Chung, M. C. Tsai, W. N. Su, C. W. Chen, B. J. Hwang, *Nanoscale* **2019**, *11*, 2710–2720.
[118] a) V. Bocharova, A. P. Sokolov, *Macromolecules* **2020**, *53*, 4141–4157; b) A. Kisliuk, V. Bocharova, I. Popov, C. Gainaru, A. P. Sokolov, *Electrochim. Acta* **2019**, *299*, 191–196.
[119] a) Y. Jiang, X. Yan, Z. Ma, P. Mei, W. Xiao, Q. You, Y. Zhang, *Polymer* **2018**, *10*, 1237; b) P. V. Wright, *Br. Polym. J.* **1975**, *7*, 319–327.
[120] A. A. Assegie, J. H. Cheng, L. M. Kuo, W. N. Su, B. J. Hwang, *Nanoscale* **2018**, *10*, 6125–6138.
[121] M. Rosso, T. Gobron, C. Brissot, J. Chazalviel, S. Lascaud, *J. Power Sources* **2001**, *97*, 804–806.
[122] B. Zhu, Y. Jin, X. Hu, Q. Zheng, S. Zhang, Q. Wang, J. Zhu, *Adv. Mater.* **2017**, *29*, 1603755.
[123] a) J. Meng, F. Chu, J. Hu, C. Li, *Adv. Funct. Mater.* **2019**, *29*, 1902220; b) L. Gao, J. Li, B. Sarmad, B. Cheng, W. Kang, N. Deng, *Nanoscale* **2020**, *12*, 14279–14289.
[124] a) R. Dallaev, T. Pisarenko, D. Sobola, F. Orudzhev, S. Ramazanov, T. Trcka, *Polymer* **2022**, *14*, 4793; b) H. Kawai, *Jpn. J. Appl. Phys.* **1969**, *8*, 975; c) M. Watanabe, M. Kanba, H. Matsuda, K. Tsunemi, K. Mizoguchi, E. Tsuchida, I. Shinohara, *Macromol. Rapid Commun.* **1981**, *2*, 741–744.
[125] a) K. Bicy, A. B. Gueye, D. Rouxel, N. Kalarikkal, S. Thomas, *Surfaces* **2022**, *31*, 101977; b) F. Zou, A. Manthiram, *Adv. Energy Mater.* **2020**, *10*, 2002508; c) Y. Wu, Y. Li, Y. Wang, Q. Liu, Q. Chen, M. Chen, *J. Energy Chem.* **2022**, *64*, 62–84.
[126] a) K. Tashiro, *Plastics* **1995**, *28*, 63–63; b) C. M. Costa, V. F. Cardoso, P. Martins, D. M. Correia, R. Goncalves, P. Costa, V. Correia, C. Ribeiro, M. M. Fernandes, P. M. Martins, S. Lanceros Mendez, *Chem. Rev.* **2023**, *123*, 11392–11487.
[127] R. Guo, H. Luo, X. Zhou, Z. Xiao, H. Xie, Y. Liu, K. Zhou, Z. Shen, L. Chen, D. Zhang, *J. Mater. Chem. A.* **2021**, *9*, 27660–27671.
[128] J. Luo, C. Fang, N. Wu, *Adv. Energy Mater.* **2017**, *8*, 1701482.
[129] Y. Kim, Y. Xie, X. Wen, S. Wang, S. J. Kim, H. Song, Z. L. Wang, *Nano Energy* **2015**, *14*, 77–86.
[130] J. Tarascon, A. Gozdz, C. Schmutz, F. Shokoohi, P. Warren, *Solid State Ionics* **1996**, *86*, 49–54.
[131] Y. Ding, P. Zhang, Z. Long, Y. Jiang, F. Xu, W. Di, *J. Membr. Sci.* **2009**, *329*, 56–59.
[132] G. Stone, S. Mullin, A. Teran, D. Hallinan, A. Minor, A. Hexemer, N. Balsara, *J. Electrochem. Soc.* **2011**, *159*, A222.
[133] a) J. Maitra, V. K. Shukla, *Am. J. Polym. Sci.* **2014**, *4*, 25–31; b) E. Kontou, G. Spathis, M. Niaounakis, V. Kefalas, *Colloid Polym. Sci.* **1990**, *268*, 636–644.
[134] R. Cross, *Am. J. Phys.* **2012**, *80*, 870–875.
[135] Z. Huang, S. Choudhury, N. Paul, J. H. Thienenkamp, P. Lennartz, H. Gong, P. Müller-Buschbaum, G. Brunklaus, R. Gilles, Z. Bao, *Adv. Energy Mater.* **2021**, *12*, 2103187.
[136] S. Wang, M. W. Urban, *Nat. Rev. Mater.* **2020**, *5*, 562–583.
[137] R. Tamate, M. Watanabe, *Sci. Technol. Adv. Mater.* **2020**, *21*, 388–401.
[138] C. Chang, Y. Yao, R. Li, Z. H. Guo, L. Li, C. Pan, W. Hu, X. Pu, *Nano Energy* **2022**, *93*, 106871.
[139] a) R. Tamate, K. Hashimoto, T. Horii, M. Hirasawa, X. Li, M. Shibayama, M. Watanabe, *Adv. Mater.* **2018**, 1802792; b) Y. Kamiyama, R. Tamate, T. Hiroi, S. Samitsu, K. Fujii, T. Ueki, *Sci. Adv.* **2022**, *8*, eadd0226.
[140] a) R. P. Sijbesma, F. H. Beijer, L. Brunsveld, B. J. Folmer, J. H. Hirschberg, R. F. Lange, J. K. Lowe, E. W. Meijer, *Science* **1997**, *278*, 1601–1604; b) I. Jeon, J. Cui, W. R. Illeperuma, J. Aizenberg, J. J. Vlassak, *Adv. Mater.* **2016**, *28*, 4678–4683; c) J. Cui, A. del Campo, *Chem. Commun.* **2012**, *48*, 9302–9304.
[141] T. Yu, T. Zhao, N. Zhang, T. Xue, Y. Chen, Y. Ye, F. Wu, R. Chen, *Nano Lett.* **2023**, *23*, 276–282.
[142] C. Bao, C. Zheng, J. Zhang, Y. Zhang, Z. You, J. Jin, H. Yuan, M. Wu, Z. Wen, *Energy Storage Mater.* **2024**, *68*, 103362.
[143] W. Cao, J. Lu, K. Zhou, G. Sun, J. Zheng, Z. Geng, H. Li, *Nano Energy* **2022**, *95*, 106983.

Manuscript received: March 29, 2024
Revised manuscript received: June 5, 2024
Version of record online: July 29, 2024